

Regulation of N₂O emissions from acid organic soil drained for agriculture

Arezoo Taghizadeh-Toosi¹, Lars Elsgaard¹, Tim J. Clough², Rodrigo Labouriau³, Vibeke Ernstsen⁴ and Søren O. Petersen¹

5 ¹ Department of Agroecology, Aarhus University, Tjele, Denmark

² Faculty of Agriculture and Life Sciences, Lincoln University, Christchurch, New Zealand

³ Applied Statistics Laboratory, Department of Mathematics, Aarhus University, Aarhus, Denmark

⁴ Geological Survey of Denmark and Greenland, Copenhagen, Denmark

Correspondence to: Arezoo Taghizadeh-Toosi (Arezoo.Taghizadeh-Toosi@agro.au.dk)

10 Abstract

Organic soils drained for crop production or grazing land are agroecosystems with potentially high, but variable emissions of nitrous oxide (N₂O). The present study investigated the regulation of N₂O emissions in a raised bog area drained for agriculture, which was classified as potentially acid sulfate soil. Here, we hypothesised that pyrite (FeS₂) oxidation was a potential driver of N₂O emissions through microbially mediated reduction of nitrate (NO₃⁻). Two sites with rotational grass, and two sites with a potato crop, were equipped for monitoring of N₂O emissions and soil N₂O concentrations at 5, 10, 20, 50 and 100 cm depth during weekly field campaigns in spring and autumn 2015. Further data acquisition included temperature, precipitation, soil moisture, water table (WT) depth, and soil NO₃⁻ and ammonium (NH₄⁺) concentrations. At all sites, the soil was acidic with pH ranging from 4.7 to 5.4. Spring and autumn monitoring periods together represented between 152 and 174 d, with cumulative emissions of 3-6 kg N₂O-N ha⁻¹ at sites with rotational grass and 19-21 kg N₂O-N ha⁻¹ at sites with a potato crop. Equivalent soil gas phase concentrations of N₂O ranged from around 10 μL L⁻¹ at grassland sites to several hundred μL L⁻¹ at potato sites, in accordance with lower soil mineral N concentrations at grassland sites. Statistical analyses using graphical models showed that soil N₂O concentration in the capillary fringe was the strongest predictor of N₂O emissions in spring and, for grassland sites, also in the autumn. For potato sites in autumn, the analysis found that NO₃⁻ availability in the top soil, together with temperature, were the main controls on N₂O emissions. Chemical analyses of intact soil cores, collected to 1 m depth at adjacent grassland and potato sites in spring and autumn, showed that the total reduction capacity of the peat soil (assessed by cerium (IV) reduction) was much higher than that represented by FeS₂, and the concentrations of total reactive iron (TRFe) were higher than those of FeS₂. Based on the statistical graphical models and the tentative estimates of reduction capacities, FeS₂ oxidation was found unlikely to be important for N₂O emissions. Possible pathways of N₂O production in spring and autumn periods, and the potential sources of N, are further discussed.

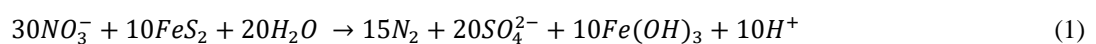
Key words: Drained peat, potentially acid sulfate soil, rotational grass, potato, nitrous oxide, reactive iron

1 Introduction

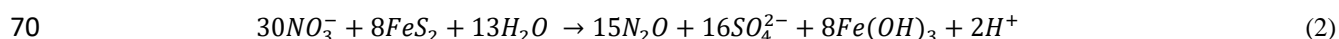
Worldwide, 25.5 million ha of organic soils have been drained for agricultural use, mainly as cropland (Tubiello et al., 2016), and this accelerates decomposition of soil organic matter and net carbon (C) and nitrogen (N) mineralisation above the water table (WT) (Schothorst, 1977). Drained organic soils are significant net sources of greenhouse gas (GHG) emissions as carbon dioxide (CO₂) and nitrous oxide (N₂O) (Goldberg et al., 2010; Maljanen et al., 2003). A recent supplement to the 2006 IPCC Guidelines for National Greenhouse Gas Inventories on Wetlands (IPCC, 2014) proposed average annual emission factors of 4.3 and 8.2 kg N₂O-N ha⁻¹ yr⁻¹ for temperate grassland on drained organic soil with low and high nutrient status, respectively, and an emission factor of 13 kg N₂O-N ha⁻¹ yr⁻¹ for cropland. For soil C losses, the emission factors proposed for the three land use categories were between 5.3 and 7.9 Mg CO₂-C ha⁻¹ yr⁻¹ (Hiraishi et al., 2014). Thus, while CO₂ emissions are overall more important, site conditions appear to be more critical for N₂O.

Site conditions are defined by land use, management, inherent soil properties and climate (Mander et al., 2010; Leppelt et al., 2014). Both WT drawdown (Aerts and Ludwig, 1997) and WT rise (Goldberg et al., 2010) may enhance N₂O emissions, but such effects depend on soil N status (Martikainen et al., 1993; Aerts and Ludwig, 1997). Maljanen et al. (2003) found that WT, CO₂ emissions and temperature at 5 cm depth explained 55% of the observed variability in N₂O emissions during a two-year field study on a drained organic soil, whereas the response to N fertilisation was limited, and they suggested that N released by soil organic matter mineralisation was the main source of N₂O. In a study comparing GHG emissions from organic soil with different land uses in three regions of Denmark (in total eight site-years), Petersen et al. (2012) also found that site conditions such as WT, pH and precipitation contributed significantly to explain N₂O emission dynamics.

In the study by Petersen et al. (2012), extremely high N₂O emissions corresponding to 38 and 61 kg N ha⁻¹ were observed from arable sites in two of the three regions investigated. Several processes can lead to N₂O formation in acid organic soil: biotic processes include ammonia oxidation by archaea or bacteria (Herrmann et al., 2012; Herold et al., 2012; Stieglmeier et al., 2014), as well as nitrifier denitrification and heterotrophic denitrification by bacteria or fungi (Liu et al., 2014; Maeda et al., 2015; Wrage-Mönnig et al., 2018). Abiotic N₂O production can occur through chemodenitrification (Van Cleemput and Samater, 1996; Jones et al., 2015) or abiotic codenitrification (Spott et al., 2011). The two regions showing extreme N₂O emissions from arable soil had both developed from marine forelands and were categorised as potentially acid sulfate soil, i.e., saturated to poorly drained soil containing pyrite (FeS₂) that, upon oxidation, may lead to acid production in excess of the soil's neutralising capacity (Madsen and Jensen, 1988). The capillary fringe of organic soils represents an interface between saturated and unsaturated soil conditions, and it was speculated that oxidation and reduction of iron sulfides could have interacted with N transformations during periods with changing groundwater level (Petersen et al., 2012). Drainage will promote oxidation of FeS₂, a process which may be linked to microbially mediated nitrate (NO₃⁻) reduction (Jørgensen et al., 2009; Torrento et al., 2010). The complete reduction of NO₃⁻ to dinitrogen (N₂) can proceed as follows:



However, in the capillary fringe residual oxygen or, alternatively, the acidification produced by FeS₂ oxidation, could favour incomplete denitrification with accumulation of the intermediate N₂O (Torrento et al., 2010):



Nitrate reduction *via* the reaction described in Eq. 2 could potentially have contributed to the very high N₂O emissions reported by Petersen et al. (2012) from the two arable sites, where groundwater sulfate concentrations were also consistently high.

75 We studied four agricultural sites within one of the regions previously studied by Petersen et al. (2012), i.e., a raised bog area with acid soil conditions. The study included two sites with rotational grass and two sites with a potato crop, and the study covered spring and autumn periods, where high emissions of N₂O occurred in previous studies (Petersen et al., 2012; Kandel et al., 2018). We hypothesised that FeS₂ oxidation coupled with NO₃⁻ reduction was a possible driver of N₂O emissions. It was further hypothesised that N₂O emissions would vary with site conditions affecting denitrification (mineral N availability, rainfall, WT depth and temperature).

80 **2 Materials and methods**

2.1 Study sites

85 The sites investigated in this study were located in Store Vildmose, which is a 5,000 ha raised bog in northern Jutland, Denmark. The area was, until 150 years ago, the largest raised bog in Denmark, and largely unaffected by human activity. The bog overlies a marine plain formed by the last marine transgression; the sea retreated around 8000 BC, and peat later developed in wet parts of the landscape, attaining a maximum depth of 4.5 to 5.3 m in central parts of the bog (Kristensen, 1945). Between 1880 and 2010, the peat has generally subsided by at least 2 m due to drainage for agriculture or peat excavation (Regina et al., 2016), and today the peat depth is mostly 1-2 m, but in some locations even less (Kandel et al., 2018). The peat and underlying sand is acidic and has been categorised as a potentially acid sulfate soil (Madsen and Jensen, 1988). According to Kandel et al. (2018), the peat at 0-25 cm depth in arable soil in 90 this area has a high degree of humification at H8 on the Von Post scale.

Four sites were selected along an east-west transect (Figure 1a). One arable site (*ARI*) was in a field cropped with second-year potato in 2015, while an adjacent site (*RGI*) in a neighbouring field had second-year rotational grass; these two sites were also represented in the study of Petersen et al. (2012) as sites *N-AR* and *N-RG*, respectively. Land use treatments (i.e., potato and rotational grass) were replicated at sites in other fields, referred to as *AR2* and *RG2*; site *AR2* 95 was located 4.6 km to the west, and site *RG2* was located 1.7 km to the east of the paired *ARI-RGI* sites (Figure 1a and S1).

2.2 Experimental design

In January 2015, an area of 10 m × 24 m was defined at the location of each site. Sampling positions were georeferenced using a Topcon HiPer SR geopositioning system (Livermore, CA). On 25 February 2015, each site was

100 fenced, and three 10 m × 8 m experimental blocks were defined (Figure 1b). Each site was further divided along its longitudinal axis to establish two 5 m × 24 m fertilisation subplots.

For monitoring of WT depth, piezometer tubes (Rotek A/S, Sdr. Felding, Denmark) were installed to 150 cm depth at the centre of each block. On either side of the piezometers, at 2.7 m distance, collars of white PVC (base area: 55 cm × 55 cm, height: 12 cm [RG] or 24 cm [AR]) were installed to between 5 and 10 cm depth (Figure 1). The higher collars
105 used at AR sites were at level with the ridges during the growth period. The collars, which were fixed to the ground by four 40 cm pegs, had a 4 cm wide flange extending outwards 2 cm from the top to support gas flux chambers. To prevent soil disturbance during gas sampling, platforms (60 cm × 100 cm) of perforated PVC were placed in front of each collar to create a boardwalk. The exact headspace of each collar was determined from 16 individual measurements of distance from the upper rim; this procedure was repeated whenever collars had been removed and reinstalled to
110 accommodate field operations.

Sets of five stainless steel diffusion probes for soil gas sampling at 5, 10, 20, 50 and 100 cm depth were installed vertically within 0.5 m of the flux measurement positions in two blocks (Block 2 and 3) at sites *AR1* and *RG1*, while at sites *AR2* and *RG2* diffusion probes were installed only in Block 2. The stainless steel probes were constructed as described in detail by Petersen (2014), with a 10 cm³ diffusion cell having a 3 mm diameter opening at the sampling
115 depth covered by a silicone membrane, which was connected to the soil surface via two 18G steel tubes with Luer Lock fittings (Figure S1).

A HOBO Pendant Temperature Data Logger (Onset Computer Corp., Bourne, MA) was installed at 5 cm depth in Block 2 at each site. A mobile weather station (Kestrel 4500; Nielsen-Kellerman, Boothwyn, PA) was mounted at 170 cm height at site *RG1* for hourly recording of air temperature, barometric pressure, wind speed and direction, and
120 relative humidity. Daily precipitation was recorded at <10 km distance from the monitoring sites at a meteorological station, from where data to fill a gap in air temperature were also obtained.

2.3 Management

Management within the fenced experimental sites followed the practices adopted by the respective farmers, e.g., with respect to fertiliser application, grass cuts, potato harvest and soil tillage. One exception to this was N fertilisation,
125 which was only given to one of the two subplots in each block (Figure 1b). Fertilised subplots of the *RG1* site received 350 kg ha⁻¹ NS 27-4 fertiliser on 16 April (DOY106), corresponding to 94.5 kg N ha⁻¹. Site *RG2* was fertilised with 20-25 Mg ha⁻¹ acidified cattle slurry (pH 6) on 5 May (DOY125), and again on 2 July (DOY183), each time corresponding to 90-110 kg total N ha⁻¹. After the second slurry application, *RG2* further received 50 kg N ha⁻¹ as NS 27-4 fertiliser, which was applied by mistake to both fertilisation subplots. The *AR1* site received 100 kg N ha⁻¹ as liquid NPS 20-3-3
130 fertiliser on 21 May (DOY141), while the *AR2* site received 110 kg N ha⁻¹ as NS 21-24 pelleted fertiliser on 30 April (DOY120). The NS fertilisers contained equal amounts of ammonium (NH₄⁺) and nitrate (NO₃⁻), while N in the NPS fertiliser was mainly as NH₄⁺.

At the *RG1* site, the grass was cut in late August, while at the *RG2* site the grass was cut in late June and on 9 September (DOY252). Potato harvest at the *ARI* site took place in mid-September (DOY 258), with interruptions due to heavy rainfall. At the *AR2* site, the potato harvest took place on 23 September (DOY266).

2.4 Field campaigns

A monitoring program was conducted during spring from 3 March (DOY63) to 16 June (DOY169), and during autumn from 3 September (DOY245) to 10 November (DOY314). Weekly measurement campaigns were conducted at each of the four sites insofar as field operations permitted. Thus, during spring there were 14, 12, 14 and 15 weekly campaigns at the *RG1*, *ARI*, *RG2*, and *AR2* sites, respectively. During autumn there were 10, 10, 7 and 10 weekly campaigns at the *RG1*, *ARI*, *RG2*, and *AR2* sites, respectively. Field trips included sampling at two sites, either *ARI* + *RG1* or *AR2* + *RG2*, and thus all four sites were visited during two field trips on consecutive days. Campaigns included registration of weather conditions and WT depth, soil sampling, soil gas sampling, and N₂O flux measurements. With few exceptions, each campaign was initiated between 9:00 and 12:00; the order of sites visited in each trip alternated from week to week.

2.4.1 Climatic conditions

Air temperature, relative humidity and barometric pressure were logged at the weather station located at *RG1*. During field campaigns, the WT depth was first determined in each of the three piezometers using a Model 101 water level meter (Solinst; Georgetown, Canada). At *ARI* and *AR2*, WT depth in Block 3 was further recorded at 30-minute time resolution for a period during autumn using MaT Level2000 data loggers (MadgeTech; Warner, NH, USA). Soil temperatures at 5, 10 and 30 cm depth were measured in each block using a high precision thermometer (GMH3710, Omega Newport, Deckenpfronn, Germany), and in addition continuous measurements of soil temperature at 5 cm depth were collected in block 2 at each site using HOBO Pendant Temperature Data Loggers (Onset Computer Corp., Bourne, MA).

2.4.2 Soil sampling

During all field campaigns, soil samples were collected separately from fertilised and unfertilised subplots by random sampling of six 20 mm-diameter cores to 50 cm depth. Each core was split into 0-25 and 25-50 cm depth, and the six subsamples from each depth were pooled. The pooled samples were transported back to the laboratory in a cooling box and stored at -20°C for later analysis of mineral N and gravimetric water content.

On 23 April (DOY113), and again on 2 September (DOY245), undisturbed soil cores (50 mm diameter, 30 cm segments) were collected to 1 m depth within 1 m distance from the positions of flux measurements in Block 3 of sites *RG1* and *ARI* (cf. Figure 1b). A stainless steel corer (04.15 SA/SB liner sampler, Eijkelkamp, Giesbeek, Netherlands) equipped with a transparent plastic sleeve was used. The steel corer's lower end was capped with a 4 cm long cutting head, and hence sampling depths were 0 to 30 cm, 34 to 64 cm and 68 to 98 cm. The intact cores were capped and sealed, and transported in a cooling box to the laboratory, where they were stored at -20°C.

2.4.3 Soil gas sampling

Soil gas samples were collected in 6 mL pre-evacuated Exetainers (Labco Ltd, Lampeter, UK) as described by Petersen (2014) and shown in Figure S2. In brief, the diffusion probes were flushed *via* the inlet tube with 10 mL N₂ containing 50 µL L⁻¹ ethylene (AGA, Enköping, Sweden) as a tracer. A three-way valve, mounted on the outlet tube, was fitted with a 10 mL glass syringe and an Exetainer. The displaced gas was collected in the glass syringe from where the soil gas sample, now partly diluted by the flushing gas, was transferred to the Exetainer. After gas sampling, the probe was flushed with 2 × 60 mL N₂ to remove ethylene, and the Luer Lock fittings were capped. Samples of the N₂/ethylene gas mixture used for sample displacement were also transferred directly to Exetainers for gas chromatographic analysis (*n* = 3) as reference for the calculation of dilution factors (Petersen, 2014). Sampling for soil gas was done in parallel with flux measurements, except when equipment had to be removed during periods with field operations. Due to damage of some probes during spring, it was decided to discontinue soil gas sampling in the unfertilised subplot at site *RG2*, which had by mistake received fertiliser on DOY 183.

2.4.4 Nitrous oxide flux measurements

Gas fluxes were measured with static chambers (60 cm × 60 cm × 40 cm) constructed from 4-mm white PVC and equipped with a closed-cell rubber gasket (Emka Type 1011-34; Megatrade, Hvidovre, Denmark) as seal during chamber deployment. Chambers were further equipped with a 12V fan (RS Components, Copenhagen, Denmark) for headspace mixing that was connected to an external battery (Yuasa Battery Inc.; Laureldale, PA), as well as a vent tube with outlet near the ground to minimise effects of wind (Conen and Smith, 1998; Hutchinson and Mosier, 1981). Also, chambers were equipped with an internal temperature sensor (Conrad Electronic SE; Hirschau, Germany), and a butyl rubber septum on top of each chamber for gas sampling. Handles attached to the top were used for straps fixing the chamber firmly against the collar. Gas samples (10 mL) were taken with a syringe and hypodermic needle immediately after chamber deployment, and then 15, 30, 45 and 60 minutes after closure. Gas samples were transferred to 6 mL Exetainer vials, leaving a 4 mL overpressure.

2.4.5 Soil analyses

Soil samples collected during the weekly campaigns were sieved (6 mm) and subsampled for determination of soil mineral N and gravimetric water content. Approximately 10 g field moist soil was mixed with 40 mL 1 M potassium chloride (KCl) and shaken for 30 min, and then filtered through 1.6 µm glass microfibre filters. Concentrations of NH₄⁺ and NO₂⁻ + NO₃⁻ in filtered KCl extracts were determined by autoanalyser (Model 3; Bran+Luebbe GmbH, Norderstedt, Germany) using standard colorimetric methods (Keeney and Nelson, 1982). Gravimetric soil water content was determined after drying of soil samples at 80°C for 48 hours.

Additional soil characteristics were determined on the intact soil cores collected in April and September at *ARI* and *RGI*. Five cm sections were subsampled from selected depths and analysed for water content, pH, electrical conductivity (EC), total soil organic C and N, and NO₂⁻. Soil pH and EC were measured with a Cyberscan PC300 (Eutech Instruments; Singapore) in a soil:water solution (1:2.5, w/v). Total soil organic C and total N were measured by

200 high temperature combustion with subsequent gas analysis using a vario MAX cube CN analyser (Elementar Analysensysteme GmbH; Langensfeld, Germany). Soil NO₂-N concentrations were analysed in soil:water extracts (1:5, w/v) using a modified Griess-Ilosvay method (Keeney and Nelson, 1982). Total organic C and total N were further determined in bulk soil samples (0-25 cm and 25-50 cm depth) collected at *RG2* and *AR2* in the same weeks as sampling of intact cores took place at *AR1* and *RG1*.

205 The concentration of total reactive Fe (TRFe) at selected depth intervals was determined in the samples from both April and September samplings of intact soil cores. The analysis of TRFe was done using a dithionite-citrate extraction (Carter and Gregorich, 2007; Thamdrup et al., 1994) followed by Fe²⁺ analysis with the colorimetric ferrozine method, which included hydroxylamine as reducing agent (Viollier et al., 2000). The extraction dissolves free (ferric) Fe oxides (except magnetite, Fe₃O₄), as well as (ferrous) Fe in FeS, but not FeS₂.

210 The intact soil cores, from the September sampling only, were further analysed for acid volatile sulfides (AVS) and chromium reducible sulfur (CRS) as indices of FeS and FeS₂, respectively. Quantification of AVS and CRS was based on passive distillation adapted from Ulrich et al. (1997) and Burton et al. (2008). Briefly, 0.5 g soil and a trap with 4 mL alkaline Zn-acetate solution (5%) was placed in 120 mL butyl-stoppered (and crimp-sealed) serum bottles, which were evacuated (1 kPa) and pressurised with N₂ (150 kPa) three times to remove O₂, eventually leaving the
215 headspace with N₂ at atmospheric pressure. Acid volatile sulfide (primarily FeS) was liberated and trapped as ZnS after injection of 12 mL anoxic 2 M HCl followed by sonication (0.5 h) and incubation (24 h) on a rotary shaker (20°C). Using the same approach with replicate soil samples, combined AVS and CRS (primarily elemental S and FeS₂) was trapped after injection of 12 mL 1 M Cr²⁺ in 2 M HCl, prepared by reduction of CrCl₃ (Røy et al., 2014). Trapped sulfide (ZnS) in the two traps was measured colorimetrically using diamine reagent (Cline, 1969), and CRS was then
220 calculated by difference.

Finally, the total reduction capacity of the peat at depths of 27-30 cm, 61-64 cm and 95-98 cm was determined. In brief, a suspension (soil:solution, 1:25; w/v) of oven dried (105°C) sieved soil (<2 mm) and 25 mM cerium (IV) sulfate reagent, Ce(SO₄)₂ in 5% sulfuric acid (H₂SO₄), was shaken horizontally for 24 h at 275 rounds per minute (rpm). After centrifugation at 2,000 rpm, residual Ce(IV) was measured by end-point titration using a solution of 5 mM FeSO₄ in 5%
225 H₂SO₄. The amount of reduced compounds was calculated and expressed as meq kg⁻¹.

2.4.6 Gas analyses

Nitrous oxide concentrations were analysed on an Agilent 7890 gas chromatograph (GC) with a CTC CombiPal auto-sampler (Agilent, Nærum, Denmark). The instrument had a 2 m back-flushed pre-column with Hayesep P connected to a 2 m main column with Poropak Q. From the main column, gas entered an electron capture detector (ECD). The carrier
230 was N₂ at a flow rate of 45 mL min⁻¹, and Ar-CH₄ (95%/5%) at 40 mL min⁻¹ was used as make-up gas. Temperatures of the injection port, columns and ECD were 80, 80 and 325°C, respectively. Concentrations were quantified with reference to synthetic air and a calibration mixture containing 2013 nL L⁻¹ N₂O. Soil profile N₂O concentrations were frequently at several hundred μL L⁻¹; linearity of the EC detector response was ascertained up to 1600 μL L⁻¹, but the

entire range was not included in analytical runs as a standard practice, and therefore the higher equivalent gas phase concentrations are relatively uncertain.

Ethylene concentrations in soil gas samples and flushing gas were analysed following a separate injection with an extended run time. All GC settings were as described above, except that run time was different, and gas from the main column was directed to a flame ionisation detector supplied with 45 mL min⁻¹ H₂, 450 mL min⁻¹ air, and 20 mL min⁻¹ N₂; the detector temperature was 200°C.

2.5 Data processing and statistical analyses

Individual N₂O fluxes were calculated in R (version 3.2.5, R Core Team, 2016) using the package HMR (Pedersen et al., 2010). This program analyses non-linear concentration-time series with a regression-based extension of the model of Hutchinson and Mosier (1981), and linear concentration-time series by linear regression (Pedersen et al., 2010). Statistical data (*p* value, 95% confidence limits) are provided by HMR for both categories of fluxes. The choice to use a linear or non-linear flux model was made based on scatter plots and the statistical output.

The temporal dynamics of N₂O fluxes were analysed using a generalised linear mixed model defined with the identity link function, the gamma distribution (see Jørgensen and Labouriau, 2012; McCullagh and Nelder, 1989), and Gaussian random components. The model contained a fixed effect representing the interaction between crop, fertilisation and sampling day, and random effects representing site and sampling position. The model for daily N₂O emission described above was used to estimate cumulative emissions by integrating the flux curves over time. Treatment effects were then analysed by specially designed linear contrasts as described in detail by Duan et al. (2017), who showed that models with untransformed responses (when using adequate distributions) allow simple statistical inference of the time-integrated N₂O emissions.

The dependence structure of variables that were potential drivers of N₂O fluxes were studied using a class of multivariate models called “graphical models” (Whittaker, 1990, see also Labouriau et al., 2008a,b; and Lamandé et al., 2011 for applications in soil science). These models represent the dependence of variables using an undirected graph (not to be confounded with the word “graph” used to refer to a plot), which is a mathematical structure composed of *vertices*, represented by points, and *edges* connecting pairs of vertices, represented by lines connecting points, according to the convention explained below. In graphical models, the variables of interest are the vertices of the graph (represented as labelled points). Here the variables used were: soil temperature at 5 cm depth (Temp5); soil temperature at 30 cm depth (Temp30); NH₄⁺ and NO₃⁻ concentrations in the top soil (AmmoniumT and NitrateT); N₂O concentration of the soil gas diffusion probe closest to, but above the WT, i.e., in the capillary fringe (N₂OWT); and finally, the N₂O flux (N₂O-flux). The dependence structure of these variables was characterised by the conditional covariances between each pair of variables given the other variables. Those conditional covariances were simultaneously estimated using the available data according to a statistical model. The graph representation of the model is constructed by connecting the pairs of vertices (i.e., pairs of variables) by an edge when the conditional correlation of the two corresponding variables, given all the other variables, is different from zero. It is possible to show that two variables directly connected in the graph carry information on each other that is not already contained in the

270 other variables (see Whittaker, 1990, Jørgensen and Labouriau, 2012). Moreover, the absence of an edge connecting two vertices indicates that (even a possible) association between the two corresponding variables can be entirely explained by the other variables. According to the general theory of graphical models, if two groups of variables, say A and B, are separated in the graph by a third group of variables, say C (i.e., every path connecting an element of A with an element of B necessarily contains an element of C), then A and B are conditionally uncorrelated given C (see Lauritzen, 1999). This property, called the separation principle, was used below to draw non-trivial conclusions on the interrelationship between N₂O-flux related variables. The graphical models were inferred by finding the model that minimised the BIC (Bayesian information criterion, i.e., a penalised version of the likelihood function) as implemented in the R package gRapHD (Abreu et al., 2010). This inference procedure yields an optimal representation of the data in the sense that the probability of correct specification of the model, when using this penalisation, tends to one as the number of observations increases (see Haughton, 1988). The confidence intervals for the conditional correlations were 280 obtained by a non-parametric bootstrap procedure (Davidson and Hinkley, 1997) with 10,000 bootstrap samples. Separate analyses were conducted for each combination of season and crop, since different dependency patterns appear in those groups.

3 Results

285 3.1 Climatic conditions

In 2015, the annual mean air temperature in the area of this study was 8.7°C, and annual precipitation was 920 mm. This was slightly above the ten-year (2009-2018) average temperature of 8.3°C, and well above the ten-year average annual precipitation of 798 mm. During the spring monitoring period, the daily mean air temperature varied between 1 and 15°C, with an increasing trend over the period, and total rainfall was 220 mm. During the autumn monitoring 290 period, the daily mean air temperature declined from 15 to 5°C, and total rainfall was 148 mm; the most intense daily rain events during spring and autumn were 16.9 and 33.2 mm, respectively.

Soil temperature at 5 cm depth showed a clear diurnal pattern (Figure S3), but at all four sites the temperature at the time of chamber deployment was close to the daily mean temperature at this depth. Thus, across the four sites the average deviation ranged from 0.2 to 0.9°C, and the largest deviations on a single day were -2.0 and 2.1°C, 295 respectively.

3.2 Soil characteristics

Soil characteristics were determined by analyses of intact cores collected in late April (DOY 113) 2015 (Table 1). At all sites the soil was acidic, with pH ranging from 4.7 to 5.4. At the paired sites *ARI* and *RGI*, a weak decline in pH was indicated at 40-50 cm depth. Electrical conductivity at *ARI* and *RGI* sites ranged from 0.15 to 0.91 mS cm⁻¹, with no 300 obvious trends in the data; the highest value (0.91 mS cm⁻¹) occurred at site *ARI* at 93-98 cm in a layer dominated by sand underlying the peat.

The organic matter composition of soil profiles at the four sites varied. Total organic C concentrations at sites *ARI* and *RG1* were 34-43% in the upper 0-40 cm, but then dropped to only 0.3-0.6% at *c.* 1 m depth in the sand. The peat was amorphous and well-decomposed at 0-20 cm depth, while the underlying peat was dominated by intact plant debris. At site *RG2*, the process of peat degradation was evident even at 0-50 cm depth, where TOC concentrations only just met the requirements for being defined as an organic soil; i.e., the organic C content was below 20 and 10% at 0-25 and 25-50 cm depth, respectively. Site *AR2* was characterised by a uniform peat layer (33-38% organic C) at 0-50 cm depth. Across all sites, the C:N ratios ranged between 14 and 26 in the organic soil layers.

Two iron sulfide fractions, as well as total reactive iron, were quantified. Acid volatile sulfide ranged from 1.7 to 4.9 $\mu\text{g S g}^{-1}$ soil across the four sites and showed no clear relationship with soil depth. This was also the case for CRS, which ranged from 24 to 155 $\mu\text{g S g}^{-1}$ dry weight soil. Total reactive Fe (TRFe) concentrations in soil profiles from sites *ARI* and *RG1* ranged from 1.19 to 4.99 mg g^{-1} dry weight soil at 0-50 cm depth, and hence concentrations of reactive Fe were up to 1500 times higher than concentrations of Fe in AVS (assuming this was FeS), and 25-120 times higher than Fe in CRS (assuming this was FeS₂). At sites *ARI* and *RG1*, TRFe declined below 20 cm depth and was close to zero in the sand below the peat layer (Table 1). The highest concentrations of TRFe at sites *RG1* (Figure 2b) and *ARI* (Figure 2d) occurred at 20 cm depth on 23 April. At site *ARI*, a sink for TRFe at 40-60 cm depth was indicated. There were only minor differences in the distribution of TRFe between seasons. There was a strong correlation between TRFe and TOC across all sites ($r = 0.88$, $n = 16$).

The total reduction capacity was determined by a wet oxidation procedure using Ce(SO₄)₂. At both *ARI* and *RG1*, the total reductive capacity of the peat at 27-30 cm depth was outside the range of the analytical method at >11,500 meq kg⁻¹. The reduction capacity dropped to around 1000 meq kg⁻¹ at 60 to 65 cm depth with a declining organic matter content, and 50 to 100 meq kg⁻¹ in the sandy layer at 100 cm depth.

3.3 Soil mineral N dynamics

Soil concentrations of NH₄⁺ and NO₃⁻ at 0-25 and 25-50 cm depth were determined in connection with field campaigns (Tables S1-S4). The residence time for mineral N in the soil solution was generally longer at *AR* compared to *RG* sites. At *AR* sites, there was an accumulation of mineral N (Table S2, S4) at both depth intervals during May, also before N fertilisation. Mineral N concentrations were greater at *ARI* compared to *AR2*, and at site *AR2* only NO₃⁻ accumulated. Fertilisation increased NH₄⁺-N and NO₃⁻-N concentrations to 100-200 $\mu\text{g g}^{-1}$ dry weight soil at all sites except *RG2* (Table S3), where acidified cattle slurry was applied. Accumulation of NO₃⁻ in the weeks after fertilisation was observed at all sites, and also there was evidence for some transport to 25-50 cm depth.

Nitrite-N concentrations were determined in soil profiles from the cores sampled at sites *RG1* and *ARI* on 23 April (DOY 113) and 2 September (DOY 245) 2015. Both fertilised and unfertilised subplots were represented, although at site *ARI* the fertilisation had not yet taken place at the time of sampling in April. There was variation at depth in the soil, which could not be explained by fertilisation. In April, the concentration of NO₂⁻-N at both sites was highest (*c.* 10

340 $\mu\text{g g}^{-1}$ dry weight soil) around 40 cm depth and declined towards the surface and deeper layers (Figure 2a,c). A decline in NO_2^- -N concentration was indicated at 50 cm depth at site *ARI* relative to site *RG1*, and also a depletion of TRFe was indicated. However, there was also a lower concentration of peat (cf. TOC in Table 1), which may account for this difference. In September, NO_2^- -N concentrations were $<1 \mu\text{g g}^{-1}$ dry weight soil at both sites, while the much higher concentrations of TRFe were comparable to those in April.

3.4 Groundwater table dynamics

345 Across the four sites, WT changes ranged from 60 to 100 cm. During spring, WT depth at sites *RG1* and *ARI* varied between 17 and 81 cm, with a steady decline until the end of April (DOY120) that was followed by a period with fluctuations around 60-80 cm depth due to frequent rainfall (Figures 3 and 4). During the first half of September (DOY246 to 259), rainfall caused the WT to rise from 80 to 40 cm depth (Figures 5 and 6). On two occasions (DOY248 and 260) the WT depth rose to 20 cm depth and only gradually declined during the following days (data not shown). From mid-September (DOY 258) then followed a period with a gradual WT decline until early November (DOY 308), where upon the WT rose from 90 to 45 cm depth during a week with intense rainfall. At site *RG2*, the WT was mostly at 50-60 cm depth during spring, with a temporary rise to 30 cm depth by 3 June (DOY139; see Figure 3). In the autumn, sampling campaigns could not be initiated until DOY260 due to harvest. By this time, the WT was close to the surface following intense rainfall, but then declined to 80-100 cm in the sandy subsoil (Figure 5). The WT at site *AR2* was consistently between 45 and 60 cm depth during spring except for a transient increase to 35 cm depth in early June (Figure 4). During autumn, the WT rose to the soil surface in September (DOY260), and then gradually withdrew until early November (DOY 307) when rainfall caused a c. 40 cm increase (Figure 6), as also observed at sites *RG1* and *ARI*.

355 3.5 Soil N_2O concentration profiles

360 The distribution and temporal dynamics of N_2O in the soil profiles showed important contrasts between grassland and arable sites. Equivalent gas phase concentrations of N_2O in passive diffusion samplers were determined concurrently with gas sampling, and results are presented as contour plots (Figures 3-6; data in Table S5). Concentrations in many cases varied by several orders of magnitude between sites and sampling days, and between depths within individual profiles, and therefore a logarithmic grey scale was used to show trends. The gaps in Figures 3-6 indicate periods, where diffusion probes could not be installed or were temporarily removed due to field operations.

365 Under the rotational grass at site *RG1*, soil N_2O concentrations during spring were mostly between 0.1 and $3 \mu\text{L L}^{-1}$ (Figure 3). A higher concentration ($15 \mu\text{L L}^{-1}$) was observed at 40-80 cm depth in the fertilised subplot around DOY139, but only in Block 3 of the field plot. At site *RG2*, the concentrations of N_2O in the soil during spring were generally similar to those of *RG1*, although there were more values in the 1 - $10 \mu\text{L L}^{-1}$ concentration range (Table S5). However, on 3 June (DOY154) a significant increase in N_2O concentration occurred in the fertilised part of the plot with a maximum of $560 \mu\text{L L}^{-1}$ at 100 cm depth (i.e., well below the WT). Soil N_2O concentrations in the unfertilised plot also increased around this time, but only to c. $15 \mu\text{L L}^{-1}$ and mainly near the soil surface.

The arable site *ARI*, with sampling positions located in a different field, but only 10-20 m from those of site *RG1*, showed very different soil N₂O concentration dynamics during spring (Figure 4). There was a consistent accumulation of N₂O at 50 and 100 cm depth where seasonal concentrations averaged 340 and 424 $\mu\text{L L}^{-1}$, respectively. In contrast, at 5, 10 and 20 cm depth the average N₂O concentrations were 10-30 $\mu\text{L L}^{-1}$, and there was no clear response to fertilisation on DOY141 in terms of soil N₂O accumulation. The soil N₂O concentrations suggested that there was considerable within-site heterogeneity in soil conditions, as the highest concentrations were observed in the unfertilised subplot. Between DOY75 and DOY100, the concentrations of N₂O peaked at nearly 1500 $\mu\text{L L}^{-1}$ at 50 cm depth and were 2-3 fold higher than at 100 cm depth. At site *AR2*, the highest soil N₂O concentrations during early spring were consistently observed at 20 cm depth, but then gradually declining to reach the background level of 0.3 $\mu\text{L L}^{-1}$ in mid-May (around DOY130). In the unfertilised field plot, the N₂O concentration then increased again at 20 cm depth to reach 272 $\mu\text{L L}^{-1}$ following rainfall, and a WT rise to 35 cm depth. With fertilisation, soil N₂O concentrations were even higher at 10 cm depth and reached nearly 400 $\mu\text{L L}^{-1}$ in mid-June.

During autumn, N₂O concentrations in the soil profile at the *RG1* and *RG2* sites varied between 0 and 12 $\mu\text{L L}^{-1}$, with a tendency for higher concentrations at 10-20 cm depth (Figure 5). At site *RG1*, where both fertilised and unfertilised subplots could be sampled, this was independent of fertilisation.

September was characterised by heavy rainfall (114 mm in total), and at site *ARI* a substantial rise in the WT from 80 to 40 cm depth was observed (Figure 6). Soil N₂O concentrations showed a dual pattern, with maxima at 10 and 100 cm depth through to DOY266 (end of September), and after this time soil N₂O rapidly declined as the WT withdrew. Nitrous oxide concentrations equivalent to several hundred $\mu\text{L L}^{-1}$ were measured even at 5 cm depth during this period. During late autumn, the N₂O concentration at 0-50 cm depth varied between 0 and 20 $\mu\text{L L}^{-1}$, whereas at 100 cm depth it remained high at 100-850 $\mu\text{L L}^{-1}$. At site *AR2*, the groundwater level was higher than at *ARI* and reached the soil surface by mid-September (DOY 260). Soil N₂O accumulated in both fertilised and unfertilised subplots following saturation of the soil, again with the highest concentrations at 20 cm depth. A secondary increase was observed near the soil surface at the last sampling on DOY314 in November, in response to a period with rainfall and a rapid WT rise.

3.6 Nitrous oxide emissions

The weekly sampling campaigns during spring and autumn showed much higher N₂O emissions at arable compared to grassland sites independent of season and fertiliser N application. At site *RG1*, N₂O emissions during spring ranged from 0 to 550 $\mu\text{g N}_2\text{O m}^{-2} \text{h}^{-1}$, with no effect of fertiliser amendment (Figure 3). The grass in the fertilised subplot showed a clear response to fertilisation that indicated uptake of fertiliser N. At site *RG2*, a peak in N₂O emissions occurred on DOY154, and the flux was still elevated at the next two samplings. This high flux coincided with the accumulation of N₂O in the soil profile described above.

At site *ARI*, the N₂O fluxes were generally much higher than at grassland sites during spring (Figure 4). Fluxes during early spring reached 2000-6000 $\mu\text{g N}_2\text{O m}^{-2} \text{h}^{-1}$ and were higher than in late spring where, as for site *RG1*, no effect of N fertilisation was observed. Hence, the higher emissions were associated with site differences other than fertilisation. The potato field at site *AR2* showed a different pattern, with N₂O fluxes remaining low during early spring, and for

several weeks after fertilisation. The highest emissions occurred, independent of fertilisation, in June following a WT
405 rise to 35 cm depth on DOY154.

In the autumn, N₂O fluxes from site *RG1* were consistently low (Figure 5). The first sampling at site *RG2* was on
DOY259 in mid-September, where a high flux of 3000 µg N₂O m⁻² h⁻¹ was seen, which dropped to near zero within 1-2
weeks. Nitrous oxide emissions at site *AR1* were high during September at 4000-10,000 µg N₂O m⁻² h⁻¹ independent of
N fertilisation (Table S2), and subsequently declined to near zero (Figure 6). High fluxes were observed on the first
410 sampling day of this monitoring period, DOY246, while WT depth was still at 40 to 80 cm depth. However, this
followed 10 and 22 mm rainfall on the previous two days. Rainfall the following days then was accompanied by a rise
in WT. The subsequent decline in N₂O emissions at *AR* sites coincided with WT withdrawal.

Cumulative N₂O emissions were calculated for the 99-105 days of monitoring in spring, and for the 47-69 d period
in autumn (Table 2). At *RG* sites, the average N₂O flux from fertilised grassland was significantly higher than from
415 unfertilised grass (7.3 vs. 2.0 kg N₂O ha⁻¹) during spring. At *AR* sites with potato, there was no significant effect of N
fertilisation, but the cumulative N₂O emissions of 15-17 kg N₂O ha⁻¹ were much higher than from *RG* sites. In the
autumn, the average cumulative emissions at the *RG* and *AR* sites were 2 and 15 kg N₂O ha⁻¹, respectively.

3.7 Interrelationships between driving variables of N₂O production

Graphical models were used to study the dependence structure among selected soil variables and N₂O fluxes.
420 Interestingly, at *RG* sites in both spring (Figure 7a) and autumn (Figure 7b), and at *AR* sites in spring (Figure 7c), the
only variable with a direct link to N₂O flux was soil N₂O concentration in the capillary fringe (N₂O_{WT}), indicating that
N₂O_{WT} carried information on the N₂O flux that could not be explained by indirect correlations between the other
variables. Moreover, the variable N₂O_{WT} separated N₂O flux from the other variables in the graph which, according to
the separation principle (an instance of the general theory of graphical models), indicates that information about this
425 variable rendered all the other variables uninformative with respect to N₂O flux. For example, in the analysis of *AR* sites
in spring (Figure 7c), the variables N₂O flux and Temp5 were not directly connected, and therefore any correlation
between Temp5 and N₂O flux could be completely explained by other variables. The only exception to this pattern was
AR sites in the autumn (Figure 7d), where instead two other variables showed a significant relationship with N₂O flux;
one variable was NitrateT, i.e., NO₃⁻-N concentration in the top soil, and the other variable was soil temperature at 30
430 cm depth. All other relationships were unrelated to N₂O flux, or could be accounted for by other variables.

4 Discussion

This study investigated seasonal dynamics of N₂O emissions and soil conditions in an area, which has been designated
as a hotspot for N₂O emissions (Leppelt et al., 2014). Spring and autumn monitoring periods together covered between
435 152 and 174 d, and cumulative N₂O emissions during these periods were in total 3-6 kg N₂O-N ha⁻¹ for rotational grass,
and 19-21 kg N₂O-N ha⁻¹ for arable sites with a potato crop. These numbers, representing <6 month periods, thus

confirmed previous results (Petersen et al., 2012) that annual N₂O emissions in this area are comparable to (*RG*), or clearly above (*AR*), the IPCC emission factors for drained organic soil of 8 and 13 kg N₂O-N ha⁻¹ yr⁻¹ for nutrient rich grassland and cropland, respectively (IPCC, 2014). The area has been characterised as potentially acid sulfate soil (Madsen and Jensen, 1988), and a previous study showed groundwater sulfate concentrations in excess of 100 mg L⁻¹ (Petersen et al., 2012). We therefore hypothesised that NO₃⁻ reduction coupled with FeS₂ oxidation could be a pathway of N₂O formation in this acid organic soil,

Pyrite, measured as CRS, was quantified at selected depths (Table 1), and with bulk density of the peat varying between 0.15 and 0.3 g cm⁻³ (data not shown), the total amount of CRS at 0 to 50 cm depth would thus be 200-350 mmol FeS₂ m⁻². The N₂O emissions observed during spring and autumn monitoring periods constituted up to 145 mmol N m⁻² in total (site *ARI*), and it is thus theoretically possible that the process described by Eq. 2 contributed to emissions of N₂O. However, the FeS₂ concentration (0.7-2.4 mmol kg⁻¹) represented a minor part of the total reduction capacity (>11,500 meq kg⁻¹ at 27-30 cm depth). Also, the concentration of total reactive Fe was 25-120 times higher than that of FeS₂ (though less in terms of reduction equivalents). Reducing agents other than FeS₂ were therefore likely to be more important, a conclusion that was later supported by a laboratory study in which peat amended with FeS₂ did not show enhanced N₂O production (Taghizadeh-Toosi et al., submitted).

4.1 Environmental drivers of N₂O emissions

The regulation of N₂O emissions was investigated using a statistical method represented by graphical models. It identified N₂O concentration in the capillary fringe as the strongest predictor of N₂O emissions from both grassland and arable soil in spring, and from grassland soil in the autumn. The implication is that N transformations at depth in the soil, and not in the top soil, were the main source of N₂O escaping to the atmosphere in these cases. In accordance with this, there was no immediate effect of N fertilisation on emissions of N₂O independent of land use. Other studies also found a limited response to fertilisation (Maljanen et al., 2003; Regina et al., 2004), although Regina et al. (2004) later observed a peak in N₂O emissions after rainfall. Goldberg et al. (2010) reported that N₂O emissions from a minerotrophic fen were produced at 30-50 cm depth, in accordance with the observations presented here, where the highest concentrations of N₂O were mostly observed at 20 or 50 cm depth (Table S5).

Peat decomposing in the capillary fringe during WT drawdown could have been the source of N for N₂O production. It is well established that N₂O emissions from organic soil may be enhanced by drainage (Martikainen et al., 1993; Taft et al., 2017), and the response will appear within days, as shown by Aerts and Ludwig (1997) in an incubation study with an oscillating WT. A stimulation of N₂O emissions by WT drawdown was also observed by Goldberg et al. (2010) when simulating drought under field conditions, although a pulse of N₂O also occurred after rewetting. In accordance with this, rising WT and/or increasing soil wetness in late spring and early autumn consistently enhanced N₂O emissions at all sites in the present study. Despite 32 mm rainfall on DOY244 and 245, the WT depth was still at 40 to 80 cm and could not account for the very high N₂O emissions observed on DOY246 (Figure 6). Well-degraded peat will release as little as 10% of its water to drainage (Rezanezhad et al., 2016). It is therefore likely that the rain was absorbed by peat above the WT and created conditions suitable for denitrification.

The increase in N₂O emissions during WT cycles reported by Aerts and Ludwig (1997) was observed only with eutrophic peat, whereas a mesotrophic peat showed no effect of WT dynamics on N₂O emissions, which were consistently low. A similar interaction between nutrient status and WT depth was observed in field studies comparing
475 N₂O emissions from minerotrophic and ombrotrophic boreal peatlands (Martikainen et al., 1993; Regina et al., 1996). In the present study, soil NH₄⁺-N and NO₃⁻-N concentrations at site *RG1* increased to 133 and 120 μg g⁻¹ dry weight soil upon fertilisation, respectively, but largely returned to the background level of around 5 and 10 μg g⁻¹ dry weight soil, respectively, within a week (Table S1). In contrast, at site *AR1* there was significant accumulation of NH₄⁺-N and NO₃⁻-N even before fertilisation on DOY141, and soil mineral N remained high for several weeks (Table S2). This
480 accumulation of soil mineral N around the time of potato crop establishment could have stimulated N₂O emissions in the arable soil. Grasslands on organic soil generally show lower emissions of N₂O compared to arable organic soil (Eickenscheidt et al., 2015), presumably because plants compete successfully with microorganisms for available N. Schothorst (1977) estimated peat decomposition indirectly from the N-content in herbage yield of grassland and concluded that the soil supplied 96 kg N ha⁻¹ when the drainage depth was 25 cm, but 160 and 224 kg N ha⁻¹ with the
485 drainage depth at 70 and 80 cm, respectively. Hence, plant uptake of N mineralised from soil organic matter above the WT likely caused the much lower N₂O emissions from rotational grass in this study.

Nitrous oxide concentration profiles provided indirect information about soil mineral N dynamics. At *RG* sites, soil N₂O concentrations were generally low and did not provide clear evidence for microbial N transformations, which supports the conclusion above that plant uptake was a main sink for the N released during peat decomposition. At site
490 *RG2* an accumulation of N₂O was seen at 1 m depth in late May (Figure 3), which could have been caused by leaching of mineral N from the acidified cattle slurry following extensive rain. In contrast, at *AR* sites there was significant accumulation of N₂O in the soil; at site *AR1* the highest concentrations occurred at 50 to 100 cm depth, while at site *AR2* the highest concentrations were at 20 cm depth, in accordance with the higher groundwater table. These observations indicated that N₂O was produced in the capillary fringe, consistent with peat decomposition as a source of
495 mineral N, and possibly also in the saturated zone (see next section). Following N fertilisation, the accumulation of N₂O in the soil profile was mostly associated with precipitation and rising WT.

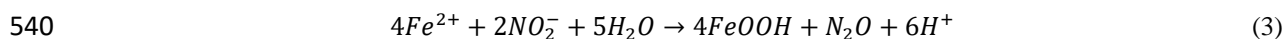
In the autumn, the graphical model identified NO₃⁻ in the top soil, and soil temperature at 30 cm depth, as significant predictors of N₂O emissions at arable sites (Figure 7). The accumulation of NO₃⁻ was much greater at site *AR1* compared to *AR2*, suggesting differences in N mineralisation potentials. It is not clear if the source of N was
500 decomposing potato crop residues or accelerated peat decomposition following soil disturbance at harvest, or both. Rainfall most likely triggered denitrification by rapidly increasing WT depth and soil water-filled pore space, thereby impeding the oxygen supply to much of the soil profile (Barton et al., 2008). This interpretation is supported by increasing N₂O concentrations below, as well as above the WT depth depending on site and block, and in fertilised as well as unfertilised subplots (Figure 6). In an annual study, conducted in other parts of the Store Vildmose bog, Kandel
505 et al. (2018) also measured high emissions of N₂O from a potato crop, i.e., around 2000 μg N₂O m⁻² h⁻¹ in October 2014 and 6000 μg N₂O m⁻² h⁻¹ in June 2015, which coincided with NO₃⁻ accumulation and rainfall. Precipitation was also high during September 2015, and the rapid rise in WT toward the soil surface resulted in accumulation of N₂O in the

top soil at all sites. However, N₂O concentrations reached only around 10 µL L⁻¹ at *RG* sites, as opposed to several hundred µL L⁻¹ at *AR* sites, confirming that soil mineral N availability was a limiting factor for N₂O emissions.

510 4.2 Pathways of N₂O emissions

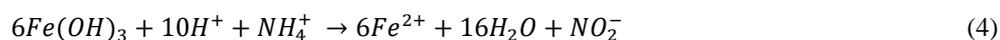
Bacterial nitrification, denitrification, and nitrifier-denitrification are all potential pathways of N₂O formation (Braker and Conrad, 2011). The significant relationship with NO₃⁻ at *AR* sites in the autumn (Figure 7) suggested that denitrification activity in the top soil controlled N₂O emissions during this period. This was different in early spring, where soil mineral N concentrations were low and N₂O accumulated near the WT depth. Here, ammonia oxidation activity may therefore have controlled N₂O emissions either directly, or indirectly *via* production of NO₂⁻ or NO₃⁻. Ammonia oxidising bacteria (AOB) are scarce in acid peat despite the presence of nitrite oxidising bacteria (NOB) (Regina et al., 1996), and some studies indicate that ammonia oxidising archaea (AOA) predominate in both abundance and activity (Herrmann et al., 2012; Stopnišek et al., 2010). Stieglmeier et al. (2014) isolated an AOA from soil that emitted N₂O at a rate corresponding to 0.09% of the NO₂⁻ produced independent of O₂ availability, but it is not known if this organism is present in acid organic soil, and at this time an indirect control of denitrification activity seems more plausible.

Stopnišek et al. (2010) found that AOA activity was not stimulated by an external source of NH₄⁺ and concluded that the activity was associated with N released from decomposing soil organic matter. The anaerobic conditions of saturated peat may have been a limiting factor for N mineralisation and therefore ammonia oxidation activity during early spring, a constraint which was alleviated as the WT declined and oxygen entered deeper soil layers. Nitrite had accumulated at 20-50 cm depth in late April at both *RGI* and *ARI* sites (Figure 2), which was consistent with peat decomposition and ammonia oxidation following WT drawdown. Total concentrations of NH₄⁺ and NO₃⁻ at 25-50 cm depth were significant (Tables S1 and S2), but well-decomposed peat is dominated by dead-end pores (Hoag and Price, 1997), and it is likely that ammonia oxidation to a large extent took place in such pores having a slow exchange of solutes with active pore volumes. The accumulation of NO₂⁻ suggested there was an imbalance between ammonia oxidation and nitrite oxidation activity. Estop-Aragonés et al. (2012) found that oxic-anoxic interfaces in peat soil were located above the WT depth, and hence the capillary fringe in this study may have been still partly anoxic. Oxygen affinity differs between nitrifiers, with AOA>AOB>NOB (Yin et al., 2018), and oxygen limitation could thus have caused the accumulation of NO₂⁻. In acid soil, this would result in product inhibition by HNO₂, if there were no mechanism to remove NO₂⁻; this would be especially true for *AR* sites, where mineral N accumulation was three to four times higher compared to *RG* sites (Tables S3-S6). Nitrifier-denitrification is one mechanism by which ammonia oxidisers can avoid HNO₂ accumulation, and this process leads to N₂O formation (Braker and Conrad, 2011). Another potential sink for NO₂⁻ is chemodenitrification, an abiotic reaction in which NO₂⁻ reacts with Fe²⁺ to produce N₂O (Jones et al., 2015):

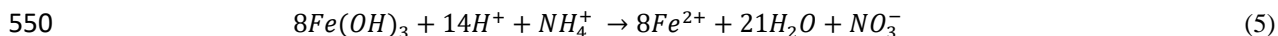


where in Eq. 3 Fe(OH)₃ is shown as anhydrous FeOOH. Some depletion of TRFe was indicated at 50 cm depth at site *ARI*, which coincided with a similar depletion in NO₂⁻ (Figure 2). Nitrifier-denitrification and chemodenitrification are both sinks for NO₂⁻, and therefore both pathways are potential sources of N₂O emissions during early spring.

545 The observation that TRFe concentrations were much higher than those of AVS or CRS (Table 1) makes it relevant to consider alternative reactions involving iron oxides/hydroxides, which have a potential to produce N₂O. One such recently described pathway is Feammox, a process whereby ammonia oxidation coupled with ferric iron reduction can produce NO₂⁻ below pH 6.5 (Yang et al., 2012):



Nitrate can also be produced under these conditions (Yang et al., 2012; Guan et al., 2018):



A shuttle of Fe²⁺ between Feammox and chemodenitrification (Eq. 3 and Eq. 4) could explain the accumulation of N₂O under anoxic conditions in the saturated zone, where presumably the availability of NH₄⁺ from peat mineralisation would be a limiting factor. The confirmation of pathways will require more detailed investigations that should include molecular analyses targeting microbial communities in the soil profile.

555

5 Conclusion

Nitrous oxide emissions were clearly higher from arable sites compared to rotational grass. This was independent of fertilisation, and instead N₂O emissions could be associated with soil N mineralisation, rainfall patterns and temperature, as hypothesized. Concentrations of pyrite were low compared to the total reduction capacity of the peat, and Fe was predominantly in forms other than pyrite. While the hypothesis, that N₂O was produced by NO₃⁻ reduction coupled with FeS₂ oxidation, could not be dismissed, it is likely that other processes were more important. There were strong seasonal dynamics in N₂O emissions, and evidence that different pathways were involved. We propose that oxidation of N mineralised from decomposing peat after WT drawdown in spring was followed by chemodenitrification (or nitrifier-denitrification), whereas in the autumn, where NO₃⁻ accumulated in arable soil after harvest, N₂O emissions were associated with rising WT and heterotrophic denitrification as the main pathway. Mitigating N₂O emissions from acid organic soil is challenged by the complexity of underlying processes. However, reducing mineral N accumulation by ensuring a vegetation cover outside the main cropping season, and stabilising the WT depth by effective drainage, are potential mitigation strategies.

570 *Author contributions.* ATT, LEL, TJ and SOP designed the study. ATT, LEL, VE and SOP carried out sampling and analyses. ATT, RL and SOP were responsible for data analyses. ATT and SOP prepared the manuscript with contributions from all co-authors.

Acknowledgements. This study received financial support from the Danish Research Council for the project “Sources of N₂O in arable organic soil as revealed by N₂O isotopomers” (DFF – 4005-00448). We would like to thank the dedicated staff involved in field campaigns, including Bodil Stensgaard, Søren Erik Nissen, Sandhya Karki, Kim

575

Johansen, Karin Dyrberg, Holger Bak and Stig T. Rasmussen. We would also like to acknowledge the support of three farmers hosting the field sites: Poul-Erik Birkbak, Rasmus Christensen and Jørn Christiansen.

580 **References**

- Abreu, G.C.G., Edwards, D., and Labouriau, R.: High-dimensional graphical model search with the gRapHD R package. *J. Stat. Softw.*, 37, 1-18, doi: 10.18637/jss.v037.i01., 2010
- Aerts, R., and Ludwig, F.: Water-table changes and nutritional status affect trace gas emissions from laboratory
585 columns of peatland soils. *Soil Biol. Biochem.*, 29, 1691-1698, doi: 10.1016/S0038-0717(97)00074-6, 1997
- Barton, L., Kiese, A., Gatter, D., Butterbach-Bahl, K., Buck, R., Hinz, C., and Murphy, D. V.: Nitrous oxide emissions from a cropped soil in a semi-arid climate. *Glob. Change Biol.*, 14, 177-192, doi: 10.1111/j.1365-2486.2007.01474.x, 2008.
- Braker, G., and Conrad, R.: Diversity, structure, and size of N₂O-producing microbial communities in soils—what
590 matters for their functioning? *Adv. Appl. Microbiol.*, 75, 33-70, doi: 10.1016/B978-0-12-387046-9.00002-5, 2011.
- Burton, E.D., Sullivan, L.A., Bush, R.T., Johnston, S.G., and Keene, A.F.: A simple and inexpensive chromium-reducible sulfur method for acid-sulfate soils. *Appl. Geochem.*, 23, 2759-2766, doi: doi.org/10.1016/j.apgeochem.2008.07.007, 2008.
- 595 Carter, M.R., and Gregorich, E.G., (Eds.): *Soil sampling and methods of analysis*, Second edition, CRC Press, USA 2007.
- Cline, J.D.: Spectrophotometric determination of hydrogen sulfide in natural waters. *Limnol. Oceanogr.*, 14, 454-458, doi: 10.4319/lo.1969.14.3.0454, 1969.
- Conen, F., and Smith, K.A.: A re-examination of closed flux chamber methods for the measurement of trace gas
600 emissions from soils to the atmosphere. *Eur. J. Soil Sci.*, 49, 701-707, doi: 10.1046/j.1365-2389.1998.4940701, 1998.
- Davidson, A.C., Hinkley, D.V.: *Bootstrap Methods and their Application*, 1st ed. Cambridge University Press, New York, NY, 1997.
- Duan, Y.F. Kong, X.-W., Schramm, A., Labouriau, R., Eriksen, J., and Petersen, S.O.: Microbial N transformations and
605 N₂O emission after simulated grassland cultivation: effects of the nitrification inhibitor 3,4-Dimethylpyrazole Phosphate (DMPP). *Appl. Environ. Microbiol.*, 83, e02019-16, doi: 10.1128/AEM.02019-16, 2017.
- Eickenscheidt, T., Heinichen, J., and Drösler, M.: The greenhouse gas balance of a drained fen peatland is mainly controlled by land-use rather than soil organic carbon content. *Biogeosciences*, 12, 5161-5184, doi: https://doi.org/10.5194/bg-12-5161-2015, 2015.
- 610 Estop-Aragonés, C., Knorr, K.-H., and Blodau, C.: Controls on *in situ* oxygen and dissolved inorganic carbon dynamics in peats of a temperate fen. *J. Geophys. Res.*, 117, G02002, doi: 10.1029/2011JG001888, 2012.
- Guan, Q.S., Cao, W.Z., Wang, G.J., Wu, F.F., Wang, C., Jiang, C., Tao, Y.R., and Gao, Y.: Nitrogen loss through anaerobic ammonium oxidation coupled with iron reduction in a mangrove wetland. *Eur. J. Soil Sci.*, 69, 732-741, doi: 10.1111/ejss.12552, 2018.

- 615 Goldberg, S.D., Knorr, K.-H., and Gebauer, G.: N₂O concentration and isotope signature along profiles provide deeper insight into the fate of N₂O in soils. *Isot. Environ. Health Stud.*, 44, 377-391, doi: dx.doi.org/10.1080/10256010802507433, 2008.
- Goldberg, S.D., Knorr, K.-H., Blodau, C., Lischeid, G., and Gebauer, G.: Impact of altering the water table height of an acidic fen on N₂O and NO fluxes and soil concentrations. *Glob. Change Biol.*, 16, 220-233, doi: 10.1111/j.1365-2486.2009.02015.x, 2010.
- 620 Haughton, D.M.A.: On the choice of a model to fit data from an exponential family. *Ann. Statist.*, 16, 342-335, doi: 10.1214/aos/1176350709, 1988.
- Herold, M.B., Baggs, E.M., and Daniell, T.J.: Fungal and bacterial denitrification are differently affected by long-term pH amendment and cultivation of arable soil. *Soil Biol. Biochem.*, 54, 25-35, doi: doi.org/10.1016/j.soilbio.2012.04.031, 2012.
- 625 Herrmann, M., Hädrich, A., and Küsel, K.: Predominance of thaumarchaeal ammonia oxidizer abundance and transcriptional activity in an acidic fen. *Env. Microbiol.*, 14, 3013-3025, doi: 10.1111/j.1462-2920.2012.02882.x, 2012.
- Hiraishi, T., Krug, T., Tanabe, K., Srivastava, N., Jamsranjav, B., Fukuda, M. & Troxler, T.: Supplement to the 2006 guidelines for national greenhouse gas inventories: wetlands. Intergovernmental Panel on Climate Change (IPCC), Geneva, Switzerland, 354 pp, 2014.
- 630 Hoag, R.S., and Price J.S.: The effects of matrix diffusion on solute transport and retardation in undisturbed peat in laboratory columns. *J Contam Hydrol* 28:193-205, 1997.
- Hutchinson, G.L., and Mosier, A.R.: Improved soil cover method for field measurement of nitrous oxide fluxes. *Soil Sci. Soc. Am. J.*, 45, 311-316, doi: 10.2136/sssaj1981.03615995004500020017x, 1981.
- 635 IPCC: 2013 Supplement to the 2006 IPCC Guidelines for National Greenhouse Gas Inventories: Wetlands, Hiraishi, T., Krug, T., Tanabe, K., Srivastava, N., Baasansuren, J., Fukuda, M. and Troxler, T.G. (eds). Published: IPCC, Switzerland, 2014.
- Jones, L.C., Peters, B., Pacheco, J.S.L., Casciotti, K.L., and Fendorf, S.: Stable isotopes and iron oxide mineral products as markers of chemodenitrification. *Environ. Sci. Technol.*, 49, 3444-3452, doi: 10.1021/es504862x, 2015.
- 640 Jørgensen, B., and Labouriau, R.: Exponential families and theoretical inference. Springer, Monografias de Matemática, Rio de Janeiro, Brazil, 2012.
- Jørgensen, C.J., Jacobsen, O.S., Elberling, B., and Aamand, J.: Microbial oxidation of pyrite coupled to nitrate reduction in anoxic groundwater sediment. *Environ. Sci. Technol.* 43, 4851-4857, doi: 10.1021/es803417s, 2009.
- 645 Kandel, T.P., Lærke, P.E., and Elsgaard, L.: Annual emissions of CO₂, CH₄ and N₂O from a temperate peat bog: Comparison of an undrained and four drained sites under permanent grass and arable crop rotations with cereals and potato. *Agric. Forest Meteorol.* 256-257, 470-481, doi: doi.org/10.1016/j.agrformet.2018.03.021, 2018.
- 650 Keeney, D.R., and Nelson, D.W.: Nitrogen-inorganic forms. In: A.L. Page, T.H. Miller and D.R. Keeney (Eds.), *Methods of Soil Analysis. Part 2. Agronomy Monographs*, 9. American Society of Agronomy and Soil Science Society of America, Madison, WI, pp. 643-692, 1982.
- Kristensen, M. K.: *Vildmosearbejdet*. Det Danske Forlag, Copenhagen, Denmark, 219 pp. (in Danish), 1945.

- 655 Labouriau, R., and Amorim, A.: Comment on ‘An Association Between the Kinship and Fertility of Human Couples’.
Science, 322 (5908):1634, doi: 10.1126/science.1161907, 2008a.
- Labouriau, R., and Amorim, A.: Human fertility increases with marital radius. *Genetics*, 178, 601-603, doi:
10.1534/genetics.107.072454 , 2008b.
- Lamandé, M., Labouriau, R., Holmstrup, M., Torp, S. B., Heckrath, G., Iversen, B. V., and Jacobsen, O.H.: Density of
macropores as related to soil and earthworm community parameters in cultivated grasslands. *Geoderma*, 162,
660 319-326, doi: doi.org/10.1016/j.geoderma.2011.03.004, 2011.
- Lauritzen, S. L.: Causal Inference from Graphical Models. In: *Complex Stochastic Systems*, O. E. Barndorff-Nielsen,
D. R. Cox and C. Klüppelberg (Editors), New York, 1999.
- Leppelt, T. Dechow, R., Gebbert, S., Freibauer, A., Lohila, A., Augustin, J., Drösler, M., Fiedler, S., Glatzel, S., Höper,
H., Järveoja, J., Lærke, P. E., Maljanen, M., Mander, Ü., Mäkiranta, P., Minkkinen, K., Ojanen, P., Regina, K.,
665 and Strömngren, M.: Nitrous oxide emission budgets and land-use-driven hotspots for organic soils in Europe.
Biogeosci., 11, 6595-6612, doi: doi.org/10.5194/bg-11-6595-2014, 2014.
- Liu, B., Frostegård, Å., and Bakken, L.R.: Impaired reduction of N₂O to N₂ in acid soils is due to a posttranscriptional
interference with the expression of nosZ. *MBio*, 5, e01383-14, doi: 10.1128/mBio.01383-14, 2014.
- Madsen, H.B., and Jensen, N.H.: Potentially acid sulfate soils in relation to landforms and geology. *Catena*, 15, 137-
670 145, doi: doi.org/10.1016/0341-8162(88)90025-2, 1988.
- Maeda, K., Spor, A., Edel-Hermann, V., Heraud, C., Breuil, M. -C., Bizouard, F., Toyoda, S., Yoshida, N., Steinberg,
C., and Philippot, L.: N₂O production, a widespread trait in fungi. *Nature Sci. Rep.*, 5, 9697, doi:
10.1038/srep09697, 2015.
- Maljanen, M., Liikanen, A., Silvola, J., and Martikainen, P.J.: Nitrous oxide emissions from boreal organic soil under
different land-use. *Soil Biol. Biochem.*, 35, 1-12, doi: doi.org/10.1016/S0038-0717(03)00085-3, 2003.
- Mander, Ü., Uemaa, E., Kull, A., Kanal, A., Maddison, M., Soosaar, K., Salm, J.-O., Lesta, M., Hansen, R., Kuller, R.,
Harding, A., and Augustin, J.: Assessment of methane and nitrous oxide fluxes in rural landscapes. *Landscape
Urban Plan.*, 98, 172-181, doi: doi.org/10.1016/j.landurbplan.2010.08.021, 2010.
- Martikainen, P.J., Nykanen, H., Crill, P., and Silvola, J.: Effect of a lowered water-table on nitrous-oxide fluxes from
680 northern peatlands. *Nature*, 366, 51-53, doi: 10.1038/366051a0, 1993.
- McCullagh, P., and Nelder, J.A.: *Generalized Linear Models*, Second Edition. Chapman and Hall/CRC, London, 1989.
- Mu, Z., Huang, A., Ni, J., and Xie, D.: Linking annual N₂O emission in organic soils to mineral nitrogen input as
estimated by heterotrophic respiration and soil C/N ratio. *PLOS ONE*, 9e96572, doi:
doi.org/10.1371/journal.pone.0096572, 2014.
- 685 Pedersen, A.R., Petersen, S.O., and Schelde, K.: A comprehensive approach to soil-atmosphere trace-gas flux
estimation with static chambers. *Eur. J. Soil Sci.*, 61, 888-902, doi: 10.1111/j.1365-2389.2010.01291.x, 2010.
- Petersen, S.O.: Diffusion probe for gas sampling in undisturbed soil. *Eur. J. Soil Sci.*, 65, 663-671, doi:
10.1111/ejss.12170, 2014.
- Petersen, S.O., Hoffmann, C. C., Schäfer, C.-M., Blicher-Mathiesen, G., Elsgaard, L., Kristensen, K., Larsen, S.E.,
690 Torp, S.B., and Greve, M.H.: Annual emissions of CH₄ and N₂O, and ecosystem respiration, from eight
organic soils in Western Denmark managed by agriculture. *Biogeosci.*, 9, 403-422, doi: doi.org/10.5194/bg-9-
403-2012, 2012.

- R Core Team: R: A Language and Environment for Statistical Computing. R Foundation for Statistical Computing. Vienna, Austria. <https://www.R-project.org/>, 2016.
- 695 Regina, K., Budiman, A., Greve, M.H., Grønlund, A., Kasimir, Å., Lehtonen, H., Petersen, S.O., Smith, P., and Wösten, H., 2015. GHG mitigation of agricultural peatlands requires coherent policies. *Clim. Policy*, 16, 522–541, doi: doi.org/10.1080/14693062.2015.1022854, 2016.
- Regina, K., Nykanen, H., Silvola, J., and Martikainen, P.J.: Fluxes of nitrous oxide from boreal peatlands as affected by peatland type, water table level and nitrification capacity. *Biogeochem.*, 35, 401-418, doi: doi.org/10.1007/BF02183033, 1996.
- 700 Regina, K., Syväsalo, E., Hannukkala, A., and Esala, M.: Fluxes of N₂O from farmed peat soils in Finland. *Eur. J. Soil Sci.*, 55, 591-599, doi: doi.org/10.1111/j.1365-2389.2004.00622.x, 2004.
- Rezanezhad, F., Price, J.S., Quinton, W.L., Lennartz, B., Milojevic, T., and Van Cappellen, P.: Structure of peat soils and implications for water storage, flow and solute transport: A review update for geochemists. *Chem. Geol.*, 429, 75-84, <http://dx.doi.org/10.1016/j.chemgeo.2016.03.010>, 2016.
- 705 Røy, H., Weber, H.S., Tarpgaard, I.H., Ferdelman, T.G., and Jørgensen, B.B.: Determination of dissimilatory sulfate reduction rates in marine sediment via radioactive ³⁵S tracer. *Limnol. Oceanogr. Methods*, 12, 196-211, doi: [10.4319/lom.2014.12.196](https://doi.org/10.4319/lom.2014.12.196), 2014.
- Schothorst, C.J.: Subsidence of low moor peat soils in the western Netherlands. *Geoderma*, 17, 265-291, doi: [doi.org/10.1016/0016-7061\(77\)90089-1](https://doi.org/10.1016/0016-7061(77)90089-1), 1977.
- 710 Schäfer, C.-M., Elsgaard, L., Hoffmann, C.C. and Petersen, S.O.: Seasonal methane dynamics in three temperate grasslands on peat. *Plant Soil*, 357, 339-353, doi: doi.org/10.1007/s11104-012-1168-9, 2012.
- Spott, O., Russow, R., and Stange, C.F.: Formation of hybrid N₂O and hybrid N₂ due to codenitrification: First review of a barely considered process of microbially mediated N-nitrosation. *Soil Biol. Biochem.*, 43, 1995-2011, doi: doi.org/10.1016/j.soilbio.2011.06.014, 2011.
- 715 Stieglmeier, M., Mooshammer, M., Kitzler, B., Wanek, W., Zechmeister-Boltenstern, S., Richter, A., and Schleper, C.: Aerobic nitrous oxide production through N-nitrosating hybrid formation in ammonia-oxidizing archaea. *ISME J.*, 8: 1135-1146, doi: [10.1038/ismej.2013.220](https://doi.org/10.1038/ismej.2013.220), 2014.
- Stopnišek, N., Gubry-Rangin, C., Höfferle, S., Nicol, G. W., Mandic-Mulec, I., and Prosser, J.I.: Thaumarchaeal ammonia oxidation in an acidic forest peat soil is not influenced by ammonium amendment. *Appl. Environ. Microb.*, 76, 7626-7634, doi: [10.1128/AEM.00595-10](https://doi.org/10.1128/AEM.00595-10), 2010.
- 720 Taft, H.E., Cross, P.A., Edwards-Jones, G., Moorhouse, E.R., and Jones, D.L.: Greenhouse gas emissions from intensively managed peat soils in an arable production system. *Agr. Ecosyst. Environ.*, 237, 162-172, doi: doi.org/10.1016/j.agee.2016.11.015, 2017.
- 725 Taghizadeh-Toosi, A., Petersen, S.O., Clough, T., and Elsgaard, L.: Nitrous oxide (N₂O) turnover in agricultural peat soil - role of nitrate, nitrite and iron sulfides. Submitted.
- Thamdrup, B., Fossing, H. and Jørgensen, B.B.: Manganese, iron, and sulfur cycling in a coastal marine sediment, Aarhus Bay, Denmark. *Geochim. Cosmochim. Acta*, 58, 5115-5129, doi: [10.1016/0016-7037\(94\)90298-4](https://doi.org/10.1016/0016-7037(94)90298-4), 1994.
- 730 Torrento C, Cama J, Urmeneta J, Otero N, and Solar A.: Denitrification of groundwater with pyrite and *Thiobacillus denitrificans*. *Chem. Geol.*, 278, 80-91, doi: [dx.doi.org/10.1016/j.chemgeo.2010.09.003](https://doi.org/10.1016/j.chemgeo.2010.09.003), 2010.

- Toyoda, S., Yoshida, N., and Koba, K.: Isotopocule analysis of biologically produced nitrous oxide in various environments. *Mass Spectrometry Reviews* 36, 135-160, doi: doi.org/10.1002/mas.21459, 2017.
- 735 Tubiello, F.N., Biancalani, R., Salvatore, M., Roissi, S., and Conchedda, G.: A worldwide assessment of greenhouse gas emissions from drained organic soils. *Sustainability*, 8, 371, 13 pp, doi: 10.3390/su8040371, 2016.
- Ulrich, G.A., Krumholz, L.R., and Suflita, J.M.: A rapid and simple method for estimating sulfate reduction activity and quantifying inorganic sulfides. *Appl. Environ. Microbiol.*, 63, 1627-1630, 1997.
- Van Cleemput, O. and Samater, A.H.: Nitrite in soils: Accumulation and role in the formation of gaseous N compounds. *Fert. Res.*, 45, 81-89, doi: doi.org/10.1007/BF00749884, 1996.
- 740 Viollier, E., Inglett, P.W., Hunter, K., Roychoudhury, A.N., and Van Cappellen, P.: The ferrozine method revisited: Fe(II)/Fe(III) determination in natural waters. *Appl. Geochem.*, 15, 785-790, doi: doi.org/10.1016/S0883-2927(99)00097-9, 2000.
- Whittaker, J.: *Graphical models in applied multivariate statistics*. John Wiley & Sons, Chichester, UK, 1990.
- 745 Wrage-Mönnig, N., Horn, M.A., Well, R., Müller, C., Velthof, G., and Oenema, O.: The role of nitrifier denitrification in the production of nitrous oxide revisited. *Soil Biol. Biochem.* 123, A3-A16, doi:doi.org/10.1016/j.soilbio.2018.03.020, 2018.
- Yang, W.H., Weber, K.A., and Silver, W.L.: Nitrogen loss from soil through anaerobic ammonium oxidation coupled to iron reduction. *Nat. Geosci.*, 5, 538-541, doi: 10.1038/ngeo1530, 2012.
- 750 Yin, Z., Bi, X., and Xu, C.: Ammonia-oxidizing archaea (AOA) play with ammonia-oxidizing bacteria (AOB) in nitrogen removal from wastewater. *Archaea Article ID 8429145*, 9 pages, doi: doi.org/10.1155/2018/8429145, 2018.

Table 1. Selected characteristics of soil profiles at the four monitoring sites with rotational grass (*RG1*, *RG2*) and potato crop (*ARI*, *AR2*). All analyses were done in triplicate; results shown represent mean and standard error of two soil profiles ($n = 2$). Soils for analyses were collected in late April except for *AVS* and *CRS* (early September). Abbreviations: EC, electrical conductivity; TOC, soil organic carbon; TRFe, total reactive iron; *AVS*, acid volatile sulfide; *CRS*, chromium reducible sulfur.

| | Depth (cm) | pH | EC | TOC (g 100 g ⁻¹) | Total N (g 100 g ⁻¹) | C:N ratio | TRFe (mg Fe g ⁻¹) | <i>AVS</i> (μg S g ⁻¹) | <i>CRS</i> (μg S g ⁻¹) |
|-------------------|---------------|-----------|-------------|---------------------------------|-------------------------------------|--------------|----------------------------------|---------------------------------------|---------------------------------------|
| <i>RG1</i> | | | | | | | | | |
| Depth 1 | 2.5-7.5 | 5.1 (0.2) | 0.26 (0.10) | 37.4 (0.2) | 1.75 (0.00) | 21.3 | 3.63 (0.11) | 2.51 (0.86) | 155 (62) |
| Depth 2 | 7.5-12.5 | 5.3 (0.1) | 0.15 (0.02) | 38.2 (0.2) | 1.79 (0.01) | 21.3 | 4.03 (0.44) | NA | NA |
| Depth 3 | 17.5-22.5 | 5.3 (0.5) | 0.37 (0.18) | 39.7 (0.3) | 1.80 (0.04) | 22.1 | 4.14 (0.32) | NA | NA |
| Depth 4 | 36-40 | 4.8 (0.1) | 0.55 (0.02) | 43.1 (2.7) | 1.85 (0.03) | 23.3 | 3.04 (0.26) | 2.60 (0.87) | 133 (64) |
| Depth 5 | 47.5-52.5 | 5.1 (0.3) | 0.42 (0.13) | 31.0 (15.6) | 1.47 (0.64) | 21.1 | 2.50 (0.55) | 4.86 (1.07) | 24 (17) |
| Depth 6 | 93-98 | 5.4 (0.0) | 0.51 (0.06) | 0.6 (0.3) | 0.01 (0.01) | ND | 0.14 (0.04) | NA | NA |
| <i>RG2</i> | | | | | | | | | |
| Depth 1 | 0-25 | 5.0 | NA | 19.8 (3.4) | 1.34 (0.13) | 14.8 | 2.29 (0.56) | NA | NA |
| Depth 2 | 25-50 | 5.1 | NA | 8.9 (3.0) | 0.63 (0.23) | 14.2 | 4.48 (NA) | 1.71 (0.00) | 33 (7.3) |
| <i>ARI</i> | | | | | | | | | |
| Depth 1 | 2.5-7.5 | 5.0 (0.1) | 0.45 (0.04) | 35.9 (0.1) | 1.81 (0.02) | 19.9 | 4.57 (0.09) | 1.74 (0.02) | 141 (9) |
| Depth 2 | 7.5-12.5 | 5.2 (0.1) | 0.42 (0.06) | 34.2 (0.2) | 1.76 (0.02) | 19.4 | 4.66 (0.15) | NA | NA |
| Depth 3 | 17.5-22.5 | 5.2 (0.1) | 0.34 (0.04) | 41.0 (2.2) | 1.93 (0.11) | 21.3 | 4.99 (0.43) | NA | NA |
| Depth 4 | 36-40 | 4.7 (0.5) | 0.37 (0.05) | 41.1 (5.8) | 1.84 (0.05) | 22.4 | 3.23 (0.41) | 2.17 (0.29) | 49 (3) |
| Depth 5 | 47.5-52.5 | 4.7 (0.3) | 0.48 (0.08) | 5.9 (1.7) | 0.37 (0.13) | 16.3 | 1.19 (0.19) | 1.98 (0.41) | 137 (39) |
| Depth 6 | 93-98 | 5.4 (0.2) | 0.91 (0.03) | 0.3 (0.1) | 0.00 (0.00) | ND | 0.18 (0.02) | NA | NA |
| <i>AR2</i> | | | | | | | | | |
| Depth 1 | 0-25 | 5.1 | NA | 33.4 (1.2) | 1.45 (0.03) | 23.1 | 4.11 (0.03) | NA | NA |
| Depth 2 | 25-50 | 5.1 | NA | 38.4 (0.2) | 1.46 (0.02) | 26.2 | 3.78 (0.14) | 1.65 (0.02) | 45 (8) |

ND – Not determined due to TOC and total N concentrations being at the limit of detection.

NA - Not analysed.

Table 2. Cumulative emissions of N₂O (kg N₂O ha⁻¹) during the spring (99-105 days) and autumn (47-69 days) monitoring period. Estimation for each season was performed using the trapezoidal approximation of the integral of the emission curve. Numbers in parentheses indicate 95% confidence intervals, and significant differences, corrected for multiple testing by the single-step method, are indicated by asterisks. *RG*, rotational grass; *AR*, arable crop (potato); F, fertilised; NF, unfertilised.

| | DOY | Cumulative N ₂ O | <i>RG-NF</i> | <i>RG-F</i> | <i>AR-NF</i> |
|---------------------------|---------|-----------------------------|--------------|-------------|--------------|
| Spring[#] | | kg ha ⁻¹ | | | |
| <i>RG-NF</i> | 63-162 | 2.0 (1.5-2.5) | | | |
| <i>RG-F</i> | 63-162 | 7.3 (4.9-9.6) | ***§ | | |
| <i>AR-NF</i> | 63-167 | 17.1 (13.9-20.2) | *** | *** | |
| <i>AR-F</i> | 63-167 | 15.0 (12.2-17.8) | *** | *** | NS |
| Autumn | | | | | |
| <i>RG-NF</i> | 252-314 | 2.0 (1.1-2.9) | | | |
| <i>RG-F</i> | 252-314 | 1.9 (1.4-2.4) | NS | | |
| <i>AR-NF</i> | 246-314 | 13.6 (10.2-17.1) | *** | *** | |
| <i>AR-F</i> | 246-314 | 15.3 (11.2-19.4) | *** | *** | NS |

§ ***, $p < 0.001$; NS, not significant ($p > 0.05$)

[#]The monitoring periods (spring and autumn) were: DOY63-162 and DOY252-314 (*RG1*); DOY64-169 and DOY260-307 (*RG2*); DOY63-162 and DOY246-308 (*AR1*); DOY64-169 and DOY245-314 (*AR2*).

Figure captions

Figure 1. A. Location of sites *ARI* and *RG1* (both at 57°13'59.7"N, 9°50'40.3E), *RG2* (57°13'55.9"N, 9°52'20.2E) and *AR2* (57°13'7.6"N, 9°46'26.9E). B. Experimental design at each of the four sites, with three blocks centered around piezometers (●) and two subplots, one of which received N fertiliser at the rate of the surrounding field. Six collars for gas flux measurements (S1-S6) were distributed as indicated, and sets of 5 diffusion probes for soil gas sampling were installed near collars in selected positions (see text).

Figure 2. Nitrite-N (a, c) and total reactive iron, TRFe (b, d), in undisturbed soil cores collected at sites *RG1* and *ARI* on 23 April (DOY113; white symbols) and 2 September (DOY245; grey symbols). Results shown are mean and standard error ($n = 2$). The dotted lines indicate WT level on the two sampling dates.

Figure 3. The top panel shows rainfall, air temperature and management (F – fertilisation) at sites *RG1* (left panels) and *RG2* (right panels) during spring, 3 March (DOY63) to 16 June (DOY169). The middle section shows N₂O fluxes (black circles; mean ± standard error, $n = 3$) and contour plots of soil N₂O concentrations in fertilised subplots, and the lower section the corresponding results for unfertilised subplots. A logarithmic grey scale was used in order to show trends within both *RG* and *AR* treatments, and between depths. Soil gas sampling positions are indicated in the contour plots; numbers shown are N₂O concentrations ($\mu\text{L L}^{-1}$). Green lines show the WT depth (which varied slightly between blocks). B2 and B3 refer to block number of diffusion probe positions.

Figure 4. The top panel shows rainfall, air temperature and management (T – tillage; F – fertilisation) at sites *ARI* (left panels) and *AR2* (right panels) during spring, 3 March (DOY63) to 16 June (DOY169). The middle section shows N₂O fluxes (black circles; mean ± standard error, $n = 3$) and contour plots of soil N₂O concentrations in fertilised subplots, and the lower section the corresponding results for unfertilised subplots. A logarithmic grey scale was used in order to show trends within both *RG* and *AR* treatments, and between depths. Soil gas sampling positions are indicated in the contour plots; numbers shown are N₂O concentrations ($\mu\text{L L}^{-1}$). Gaps are indicated where soil gas sampling probes were installed late, or removed due to field operations. Green lines show the WT depth (which varied slightly between blocks). B2 and B3 refer to block number of diffusion probe positions.

Figure 5. The top panel shows rainfall, air temperature and management (H - harvest) at sites *RG1* (left panels) and *RG2* (right panels) during autumn, 3 September (DOY245) to 10 November (DOY314). The middle section shows N₂O fluxes (black circles; mean ± standard error, $n = 3$) and contour plots of soil N₂O concentrations in fertilised subplots, and the lower section the corresponding results for unfertilised subplots. A logarithmic grey scale was used in order to show trends within both *RG* and *AR* treatments, and between depths. Soil gas sampling positions are indicated in the contour plots; numbers shown are N₂O concentrations ($\mu\text{L L}^{-1}$); the probes were absent in the unfertilised subplot after harvest. Green lines show the WT depth (which varied slightly between blocks). B2 and B3 refer to block number of diffusion probe positions.

Figure 6. The top panel shows rainfall, air temperature and management (H - harvest) at sites *ARI* (left panels) and *AR2* (right panels) during autumn, 3 September (DOY245) to 10 November (DOY314). The middle section shows N₂O

fluxes (black circles; mean \pm standard error, $n = 3$) and contour plots of soil N₂O concentrations in fertilised subplots, and the lower section the corresponding results for unfertilised subplots. A logarithmic grey scale was used in order to show trends within both *RG* and *AR* treatments, and between depths. Soil gas sampling positions are indicated in the contour plots; numbers shown are N₂O concentrations ($\mu\text{L L}^{-1}$). Green lines show the WT depth (which varied slightly between blocks). B2 and B3 refer to block number of diffusion probe positions.

Figure 7. Using graphical models, a statistical analysis was conducted for each combination of crop (*RG*, *AR*) and season (spring, autumn). a. *RG*, spring; b. *RG*, autumn; c. *AR*, spring; and d. *AR*, autumn. The edges (“lines”) connecting vertices (“points”) indicate significant relationships between explanatory variables and the response variable (N₂O flux). Statistical results for effects on N₂O flux are: [1] 2.32 (0.12-9.11, $p = 0.011$); [2] 0.74 (0.06-3.05, $p = 0.034$); [3] 0.78 (0.41-2.47, $p = 0.0002$); [4] 1.34 (0.78-4.08, $p = 0.008$); and [5] 2.45 (1.10-9.90, $p = 0.0002$). Key to variables: AmmoniumT – NH₄⁺ at 0-25 cm depth; NitrateT – NO₃⁻ at 0-25 cm depth; N₂O WT – equivalent soil gas phase concentration closest to, but above the water table depth; Temp5 – soil temperature at 5 cm depth; Temp30 – soil temperature at 30 cm depth.

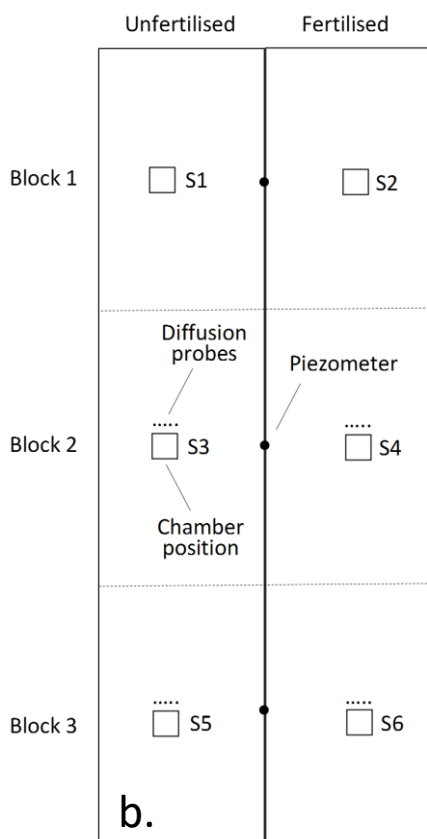


Figure 1

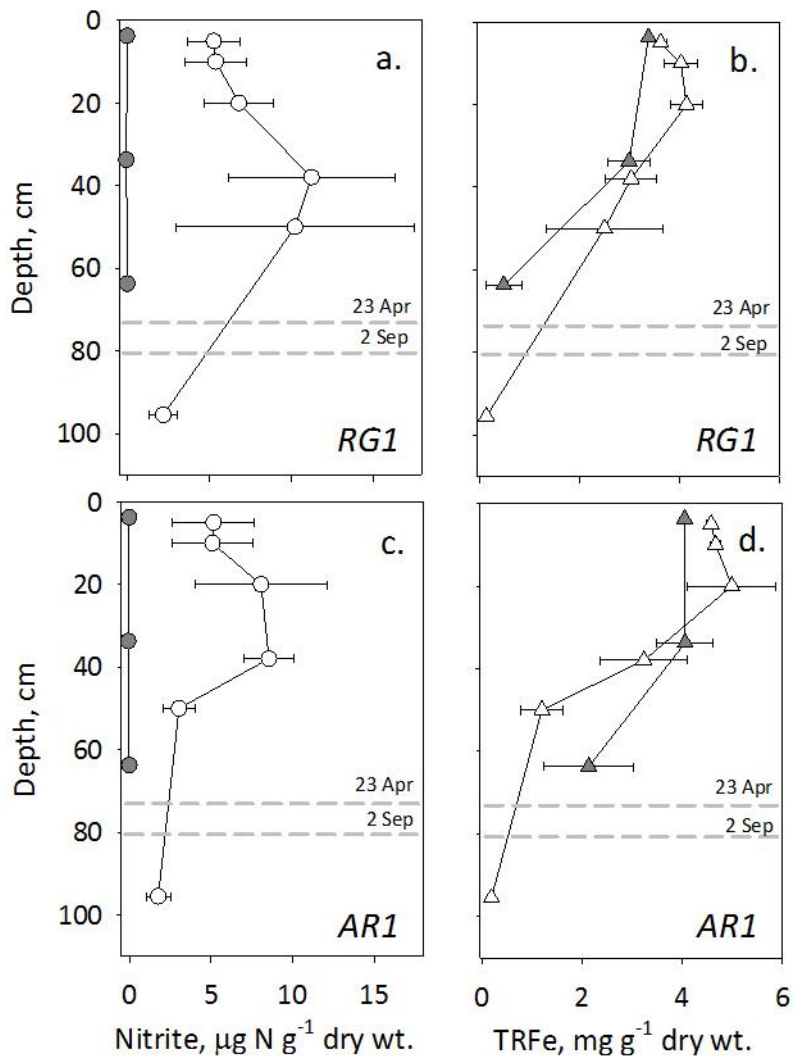


Figure 2.

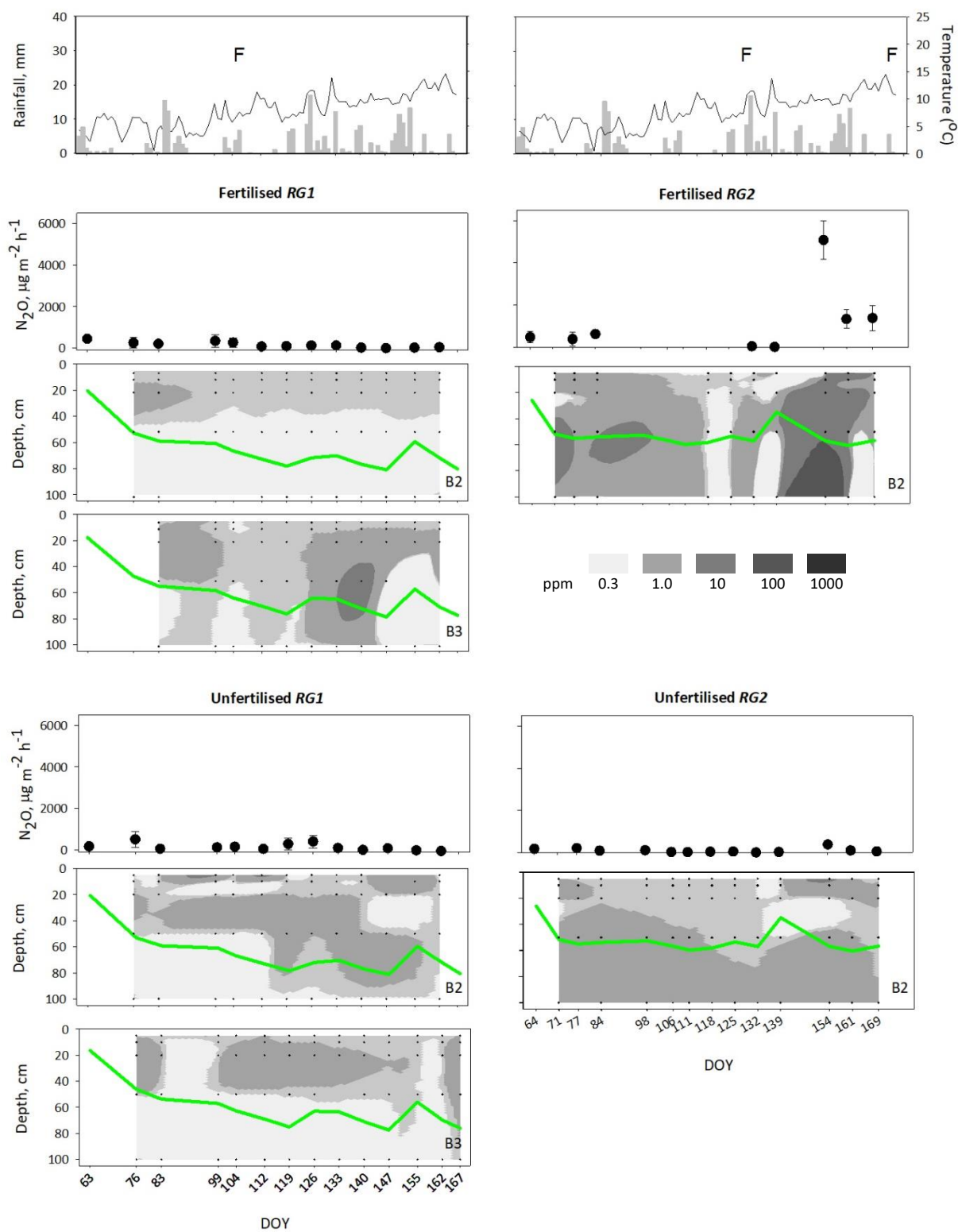


Figure 3

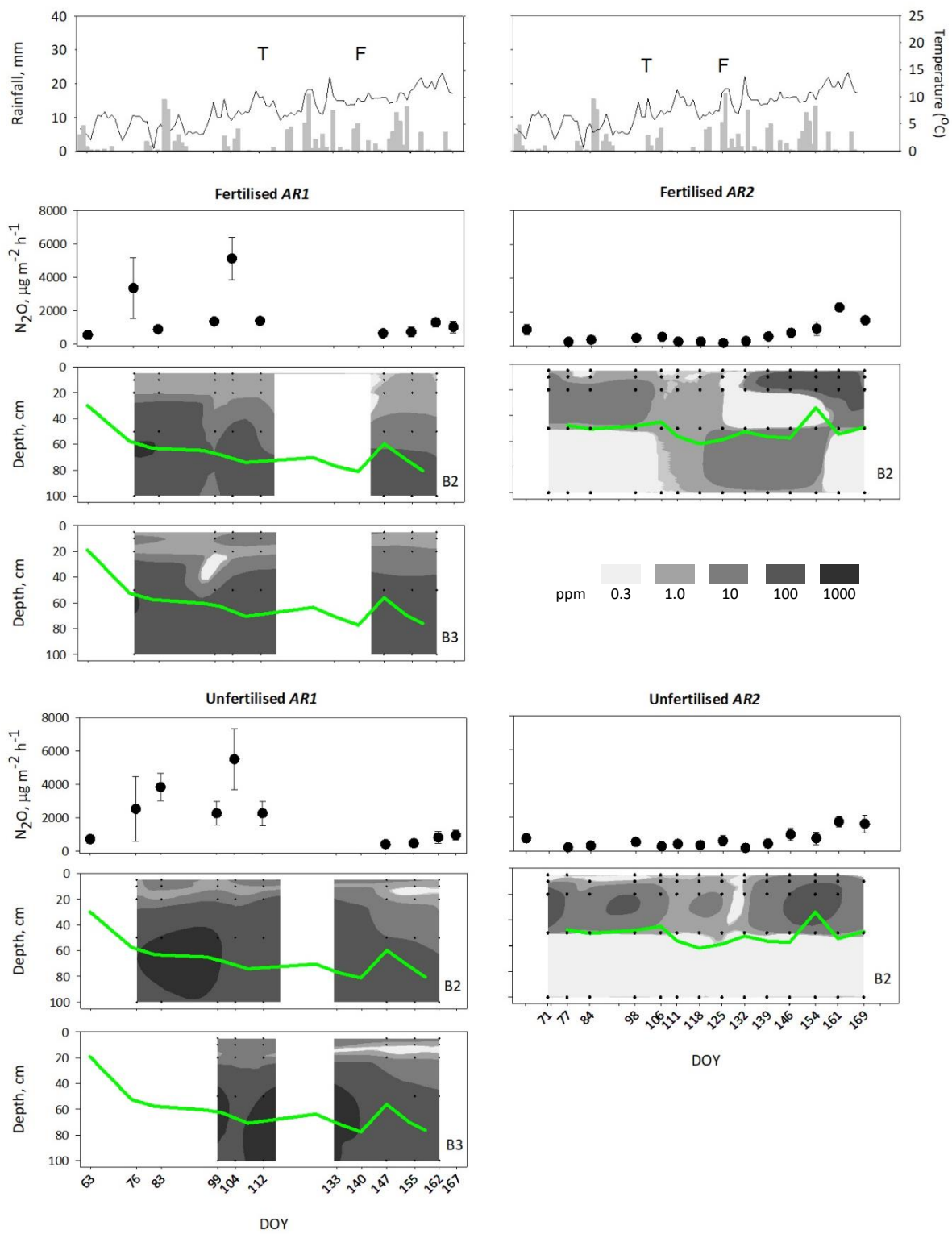


Figure 4

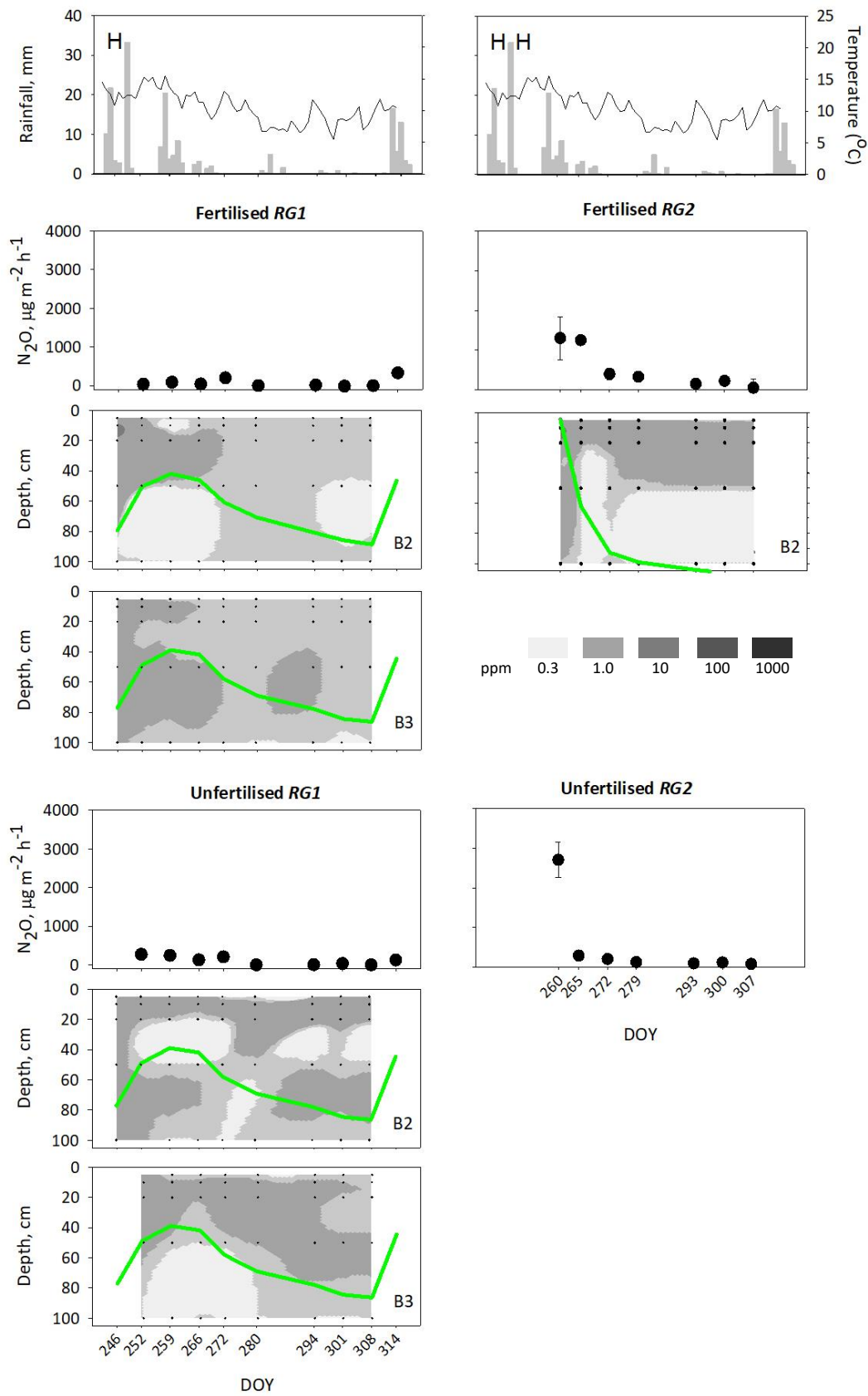


Figure 5

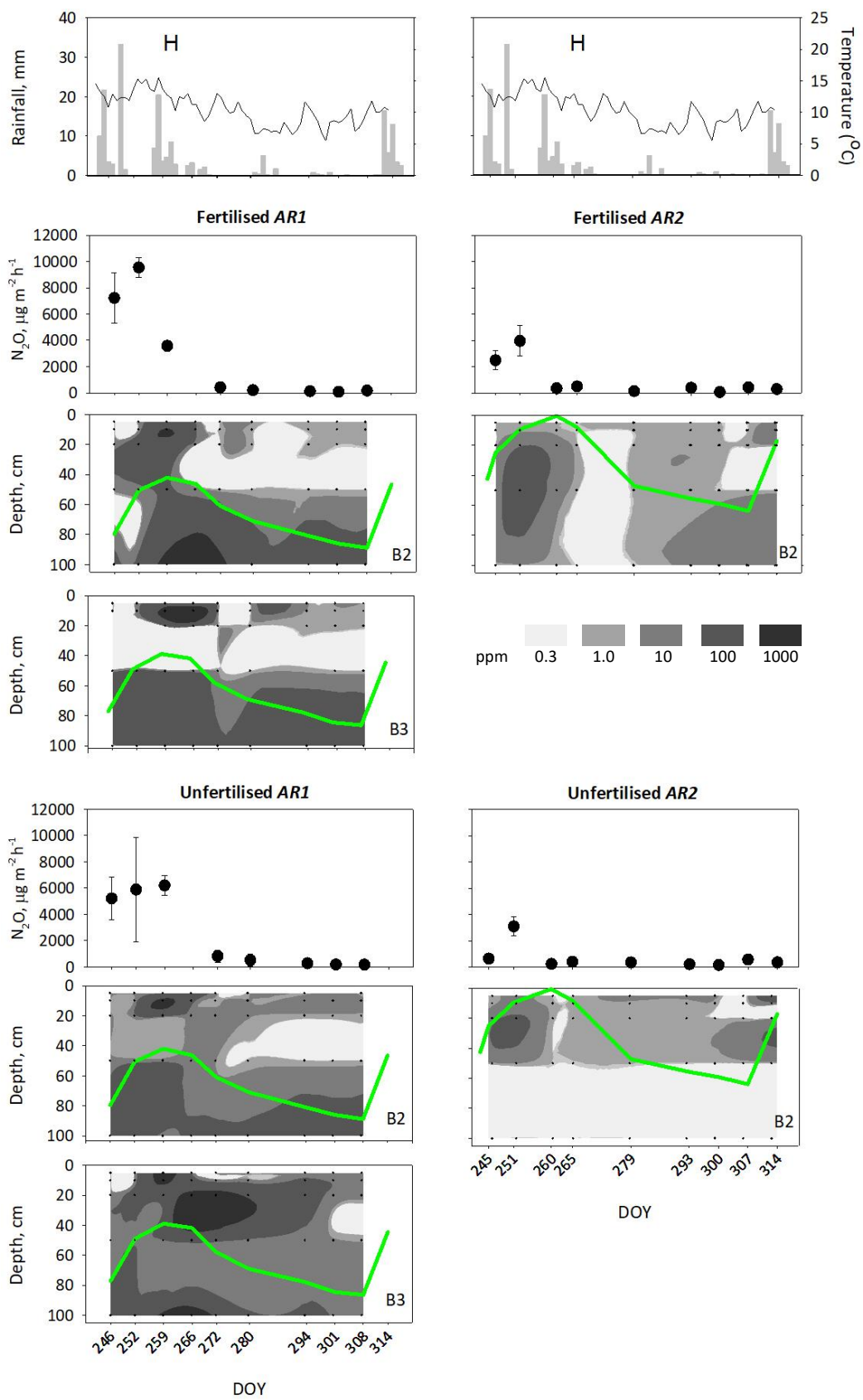


Figure 6

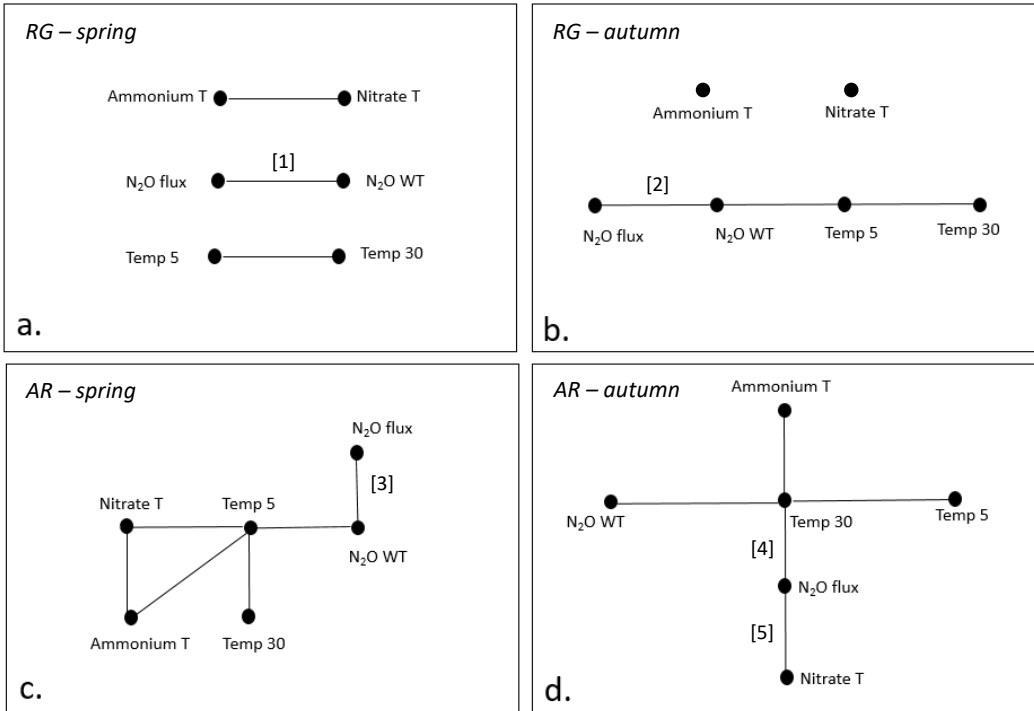


Figure 7